NTNU
Norwegian University of
Science and Technology

Adsorption of CO on nickel-decorated muscovite mica

Anna Tiseth Støvneng

Master of Science
Submission date: May 2018
Supervisor: Steinar Raaen, IFY

Norwegian University of Science and Technology
Department of Physics

Abstract

Adsorption of carbon monoxide on nickel-decorated muscovite mica is studied using the surface analysis techniques X-ray photoelectron spectroscopy, temperature programmed desorption, and atomic force microscopy.

Muscovite mica is a clay mineral that forms large crystalline flakes and is therefore well suited for surface analysis studies. The mica samples are decorated with various amounts of nickel, making a system that can serve as a model for various catalytic processes. Carbon monoxide is known not to adsorb on clean mica surfaces, but adsorbs readily when nickel is evaporated onto the mica surface.

Three main desorption peaks for carbon monoxide are found, around 250-280 K, 350-420 K and 550-600 K. The number of peaks, and their intensities depend on the amount of nickel deposited on the mica surface, and on the way the samples are prepared. Kinetic desorption parameters are found for the different samples, with desorption energies ranging from 0.1 to 1.25 eV depending on nickel amount and CO coverage. The corresponding pre-exponential factors are found in a range from 1 to $10^{8.5}$ s^{-1}, indicating that the CO desorption is not of first order for any of the samples.

The results show that the sample preparation procedure is of importance for CO adsorption, especially the annealing procedure. Mica surfaces annealed at 700 K overnight, prior to Ni and CO exposures at substrate temperatures of 150 K were found to adsorb the largest amounts of CO.

XPS measurements show some evidence of CO decomposition on our samples. A small increase in the carbon peak is found for some of the samples after CO adsorption and desorption. Comparing this to earlier studies, this carbon might desorb if the surfaces are exposed to oxygen prior to desorption, at temperatures around 620 K and 820 K.

Sammendrag

Adsorpsjon av karbonmonoksid på nikkeldekorerte muskovittprøver studeres ved hjelp av ulike teknikker for overflateanalyse. De ulike teknikkene brukt er røntgenfotoelektronspektroskopi, temperaturprogrammert desorpsjon og atomkraftmikroskopi.

Muskovitt er et leirmineral som man finner i store krystallinske flak, og det egner seg derfor godt for overflatestudier. Muskovittprøvene er dekorert med ulike mengder nikkel, slik at det utgjør et system som kan fungere som en modell for ulike katalytiske prosesser. Det er kjent at karbonmonoksid ikke adsorberer på en ren muskovittoverflate, men at det adsorberer når overflaten er dekorert med nikkel.

Tre hoveddesorpsjonstopper for karbonmonoksid er funnet, i områdene 250-280 K, 350-420 K og 550-600 K. Antall topper og deres intensitet avhenger av mengde nikkel på overflaten, og av hvordan prøvene er preparert. Kinetiske parametere er funnet for de ulike prøvene, med desorpsjonsenergier fra 0.1 til 1.25 eV, avhengig av nikkelmengde og karbonmonoksiddekning. De tilhørende prefaktorene er funnet å være fra 1 til $10^{8.5}$ s^{-1}, noe som indikerer at desorpsjonen ikke er av første orden for noen av prøvene.

Resultatene viser at prøvepreparingen er viktig for adsorpsjon av karbonmonoksid. Dette viser seg spesielt for utgassingen av prøven. Muskovittoverflatene som ble utgasset ved 700 K over natten, før Ni og CO-eksponering ved 150 K er funnet å adsorbere mest karbonmonoksid.

XPS-målinger tyder på at CO brytes ned til oksygen og karbon på prøvene. En liten økning i karbon er funnet på noen av prøvene etter CO adsorpsjon og desorpsjon. Ved å sammenligne dette med tidligere studier, kan man anta at rekombinert CO vil desorbere dersom overflatene eksponeres for oksygen før desorpsjon, ved temperaturer rundt 620 K og 820 K.

Preface

This work is a continuation of the work done on my specialisation project, which was carried out during the autumn of 2017. Most of the work included in this thesis is carried out during the spring of 2018, at Steinar Raaen's laboratory at NTNU, Trondheim.

I would like to thank Professor Steinar Raaen and PhD candidate Kristoffer Hunvik for great help and guidance in both my work in the laboratory and in the writing of the thesis. I would also like to thank Barbara Pacáková for a great introduction to the atomic force microscope.

Anna Tiseth Støvneng

May 2018

Trondheim

Contents

1 Introduction

1.1 Motivation and background

There are many reasons for studying adsorption on different surfaces, and one important reason is the reduction of greenhouse gases in the world. Fossil fuels supply more than 98 % of the world's energy needs, and the combustion of fossil fuels is one of the major sources of the greenhouse gas CO_2 [1]. It is therefore necessary to develop technologies that will allow the world to utilise the fossil fuels, but at the same time reducing the emission of greenhouse gases. A range of possibilities lie in the development of e.g. CO_2 capture and production of clean fuels.

It has been shown that clay may adsorb substantial amounts of carbon dioxide, which may be of considerable interest to problems related to the environment and climate change [2, 3]. Also, a lot of catalytic reactions involving CO are being studied for the production of clean fuel, carbon capture and energy storage. A recent study has found that Ni-mica catalysts exhibit high catalytic activity and long-term stability for ammonia decomposition to CO_x-free H_2, so that H_2 can be used as a clean fuel [4]. Other studies have shown that nickel supported catalysts are effective for CO methanation, which can be useful for carbon capture, energy storage and production of synthetic natural gas for use in biofuels [5, 6]. With this in mind, the adsorption of carbon monoxide on nickel-decorated muscovite mica is studied. Muscovite mica is an ideal clay material, as it can be easily cleaved, it is available in high-grade natural and synthetic forms, and shows reasonable thermal stability up to 900 K [7].

When doing experiments on adsorption, it is important to have a good knowledge of the substrate material's surface. This is due to the fact that most forms of solid matter exhibit a surface layer which is different from that of the underlying material [8]. In this work, X-ray photoelectron spectroscopy (XPS), temperature programmed desorption (TPD), and atomic force microscopy (AFM) have been used to analyse the surface of nickel-decorated muscovite mica and the adsorption of carbon monoxide on these surfaces.

1.2 Structure of the report

Chapter 2 includes theory about the material used in this work and theory on the growth of thin films on a material. The experimental techniques used,

including XPS, TPD, AFM and sample preparation, will be presented in chapter 3. The results will be presented in figures and tables in chapter 4 along with some comments, before being discussed in more detail in chapter 5. Chapter 6 includes concluding remarks as well as some thoughts about further work on this system.

2 Theory

2.1 Muscovite mica

Muscovite mica is the most common mineral of the mica family [9]. It is known for its large, atomically flat, and chemically inert surfaces produced by perfect cleavage in the (001) plane. The clay mineral is easily found in nature, or it can be obtained synthetically.

2.1.1 Structure

Muscovite mica is a monoclinic silicate, and it has the chemical composition $KAl_2(Si_3AlO_{10})(OH)_2$. Its structure is presented in figure 2.1.

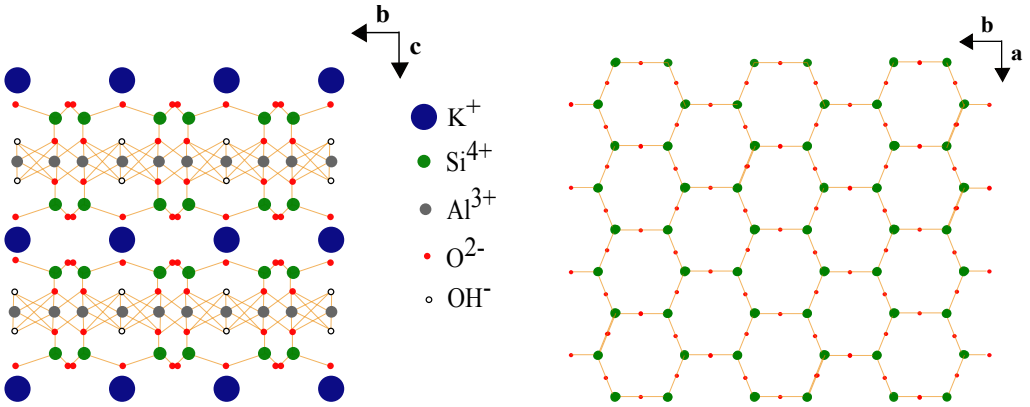

(a) Side-view of the structure

(b) Hexagonal arrangement of the (001) surface top layer

Figure 2.1: The structure of muscovite mica. (a) Side-view of the structure, showing aluminosilicate layers separated by electrostatically bound interlayer potassium ions. (b) Hexagonal arrangement of the (001) surface top layer, showing Si and O atoms of a cleaved mica surface. The figures are adapted from [9].

As seen in figure 2.1a, the structure consists of three layers. There are two identical tetrahedral layers, with the composition $(Si, Al)_2O_5$ and with the vertices pointing inward. Between these layers is a layer of octahedrally coordinated metal atoms, mostly aluminium. This aluminosilicate sheet has a negative charge, which comes from a substitution of a quarter of the Si^{4+} ions by Al^{3+} ions. Compensating for this charge is an interlayer of electrostatically bound potassium ions (K^+), which keeps the aluminosilicate sheets together. The muscovite mica is easy to cleave in the (001) plane, and this is due to the

weak bonds between the potassium ions and the two adjacent aluminosilicate sheets. When cleaved, the atomic structure of the aluminosilicate sheets is undisturbed while the potassium layer is disrupted. This makes the cleaved surface reveal a hexagonal arrangement of Si (partly Al) and O atoms, which is presented in figure 2.1b.

2.2 Nickel on muscovite mica

Earlier work has shown that CO does not adsorb on clean muscovite mica surfaces, and this is in agreement with other articles on the subject [7, 10]. It is however shown that CO does adsorb, both on different nickel surfaces [11–14] and on nickel-decorated muscovite mica [10]. To develop an understanding of the adsorption of CO on nickel-decorated mica surfaces, it is necessary to discuss how nickel may grow on the muscovite mica surface.

2.2.1 Growth modes

There are three different modes of crystal growth which are thought to occur on surfaces in the absence of surface defects or interdiffusion [15]. These crystal growth modes are illustrated in figure 2.2. The crystal growth mode illustrated in (a) is called the layer mode, or the Frank-van der Merwe mode. The atoms in the layer are more strongly bound to the substrate than to each other, so that they form a complete monolayer on the surface. The next layer will be less tightly bound to the surface. The crystal growth mode illustrated in (c) is called the island mode, or the Volmer-Weber mode. Small clusters are nucleated directly on the substrate surface and then grow into islands of the condensed phase, because the atoms/molecules of the deposit are more strongly bound to each other than to the substrate. The last one, illustrated in (b), is the intermediate case, which is called the layer plus island mode, or the Stranski-Krastanov mode. After the first one or more monolayers are formed, the subsequent layer growth is unfavourable and islands are formed on top of the layers. Almost any factor disturbing the monotonic binding energy, characteristic for layer growth, can be the cause for this.

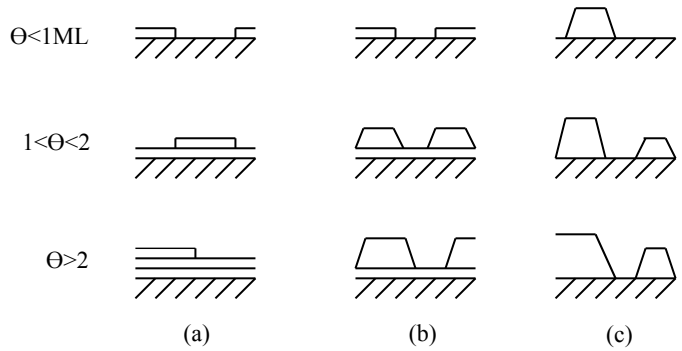

Figure 2.2: Schematic of different growth modes. (a) The layer mode, also called the Frank-van der Merwe mode. (b) The layer plus island mode, also called the Stranski-Krastanov mode. (c) The island mode, also called the Volmer-Weber mode. The growth modes are illustrated in three different cases with respect to the amount of monolayers, Θ. The figure is adapted from [15].

The Ni-mica system obeys the Volmer-Weber growth mode (island mode), due to the weak bindings between nickel and mica [16, 17]. This gives ground for several different adsorption sites, e.g. the interface between the mica substrate and the nickel islands, or at different sites on the nickel islands, given that there is no adsorption on the mica substrate itself.

3 Experimental techniques

This chapter includes brief explanations of the techniques used in this work. First the techniques X-ray photoelectron spectroscopy (XPS), temperature programmed desorption (TPD), and atomic force microscopy (AFM), will be presented in sections 3.1 to 3.3. Both XPS and TPD rely on ultra high vacuum conditions, which is explained in section 3.4. The last part of the chapter, section 3.5, will include the methods used in the preparation of the sample.

3.1 X-ray photoelectron spectroscopy (XPS)

XPS is one of the most common photoelectron spectroscopy techniques, which utilises the photoelectric effect. The main aim of the technique is to define the elemental composition of the outer 1-10 nm of any solid substrate, and it detects any element except hydrogen and helium. It is a popular technique because of the high information content of the scans, the flexibility in addressing a wide variety of samples, and its sound theoretical basis [18].

In short, the surface which is analysed is placed in a vacuum environment and irradiated with photons from an X-ray source [18]. Atoms at the surface of the material emit photoelectrons after a direct transfer of energy from the photon to the core-level electron. The emitted photoelectrons are separated according to energy, and then counted. The number of electrons emitted is related to the concentration of the emitting atom in the sample.

3.1.1 Basic principles

The main aspect of XPS is the production of photoelectrons. When a photon strikes an atom, one of three events may occur: the photon can pass through with no interaction, the photon can be scattered by an atomic orbital electron leading to partial energy loss, or the photon may interact with an atomic orbital electron with total transfer of the photon energy to the electron, leading to electron emission from the atom [18]. The latter event is the basis of the XPS technique.

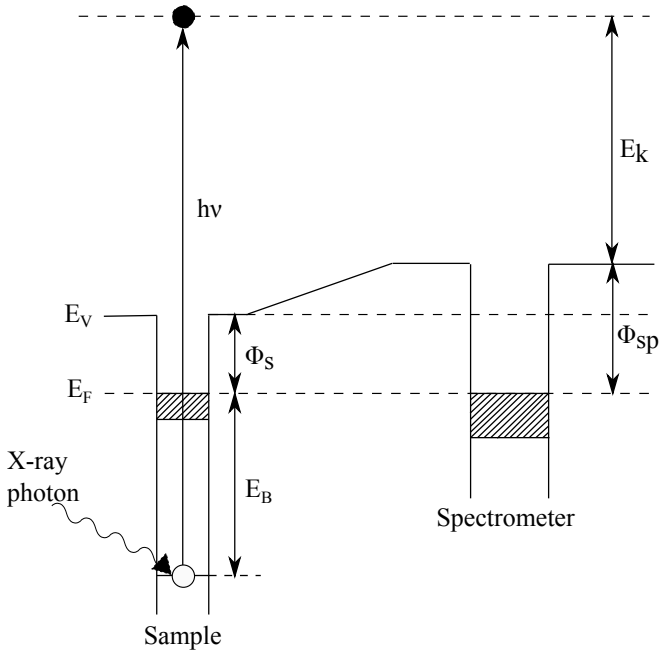

Figure 3.1: Schematic diagram of the photoemission process. The sample is irradiated with X-rays of energy $h\nu$, and electrons of binding energy E_{B} are ejected. The electrons have kinetic energy E_{k}, which can be measured by the spectrometer. Φ_{s} is the work function of the sample, and Φ_{sp} is the work function of the spectrometer. Figure is adapted from [19].

The kinetic energy of the emitted electrons is given by

$$E_{\mathrm{k}} = h\nu - E_{\mathrm{B}} - \Phi_{\mathrm{sp}}, \tag{3.1}$$

where $h\nu$ is the energy of the X-ray source, E_{B} is the binding energy of the electron in the atom, and Φ_{sp} is the spectrometer work function, a combination of the sample work function Φ_{s} and the work function induced by the electron energy analyser [19]. The process is shown in an energy level diagram in figure 3.1. The work function of the sample defines the minimum energy required to remove an electron from a solid, while the work function of the analyser gives the energy the photoelectrons need to be detected by the analyser (see section 3.1.3). Compensating for the work function electronically, the kinetic energy is given by

$$E_{\mathrm{k}} = h\nu - E_{\mathrm{B}}. \tag{3.2}$$

In XPS, the measured quantity is the kinetic energy, and combining this with the known value of the energy of the X-ray source, the binding energy E_{B} is easily obtained. The electron binding energy is defined as the extent

of the attraction with which the electrons are bound to atoms/ions through electromagnetic forces [18]. For the photoelectrons to be ejected, $E_B < h\nu$.

In addition to the production of photoelectrons in XPS, Auger electrons are also produced, and these can also appear in the XPS spectrum. The two processes are illustrated in figure 3.2. The photon from the X-ray source will transfer energy to a core-level electron, which leads to photoemission from the N-electron initial state [18]. The atom, now in an (N-1)-electron state, can then reorganise by dropping an electron from a higher energy level to a vacant core hole, which leads to the emission of an Auger electron. The Auger electrons differ from the photoelectrons, as the Auger electron energy is independent of the irradiation energy.

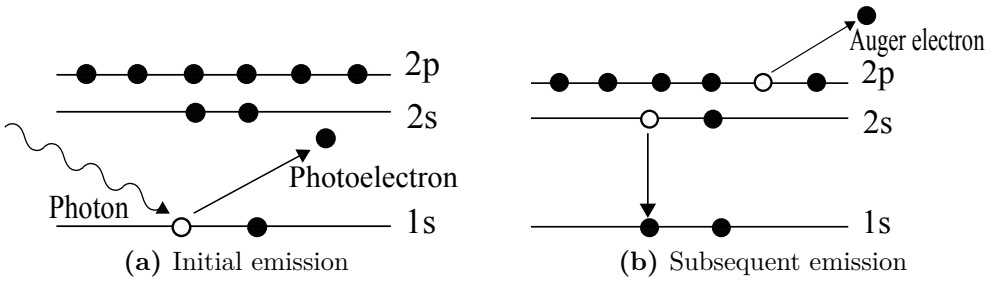

(a) Initial emission **(b)** Subsequent emission

Figure 3.2: Illustration of the processes of producing (a) photoelectrons and (b) Auger electrons. The emission of photoelectrons is the initial emission and the emission of Auger electrons is the subsequent emission.

The XPS spectrum

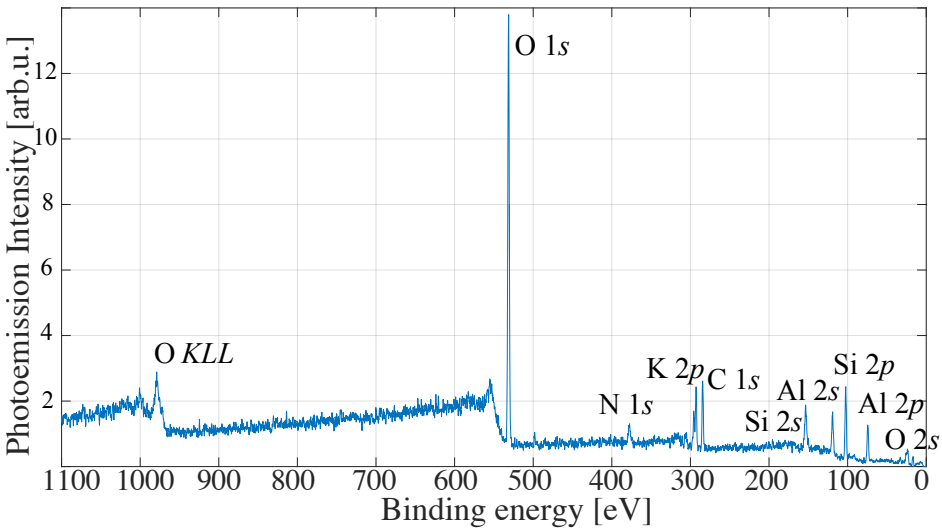

Figure 3.3: A typical XPS survey scan of a sample of untreated muscovite mica.

The XPS spectrum is generated by plotting the measured photoelectron intensity as a function of the binding energy E_B, as shown in figure 3.3. The binding energies of the lines in the spectrum are a direct representation of the atomic orbital energies. Using tables of photoelectron binding energies for all elements, the peaks in the spectrum can be assigned to different elements [19]. Figure 3.3 shows a typical survey spectrum of a sample of untreated muscovite mica, and the different elements identified in the sample are given.

For the p, d and f peaks, two peaks will be observed in the spectrum. This is seen in the survey spectrum in figure 3.3, where e.g. the O $1s$ peak is one clear peak, while the K $2p$ peak has two distinct peaks. The K $2p$ peaks are also presented in figure 3.4, which shows a core-level scan of the K $2p$ peaks in the muscovite mica sample.

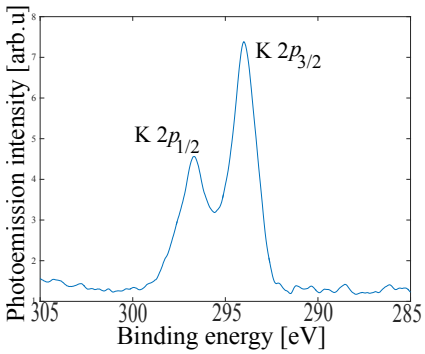

Figure 3.4: K $2p$ peaks.

The doublets are due to spin-orbit splitting. The spin angular momentum, S, and the orbital angular momentum, L, can combine in different ways and produce new states that are characterised by the total electronic angular momentum, $J =\mid L \pm S \mid$, where $S = 1/2$ and $J = 1/2, 3/2, 5/2, ...$ [18]. As for the potassium peaks, the $2p$ state has $L = 1$, which gives $J = 1/2$ and $J = 3/2$. The peak is then split into K $2p_{1/2}$ and K $2p_{3/2}$, with area ratio 1:2.

Electron inelastic mean free path

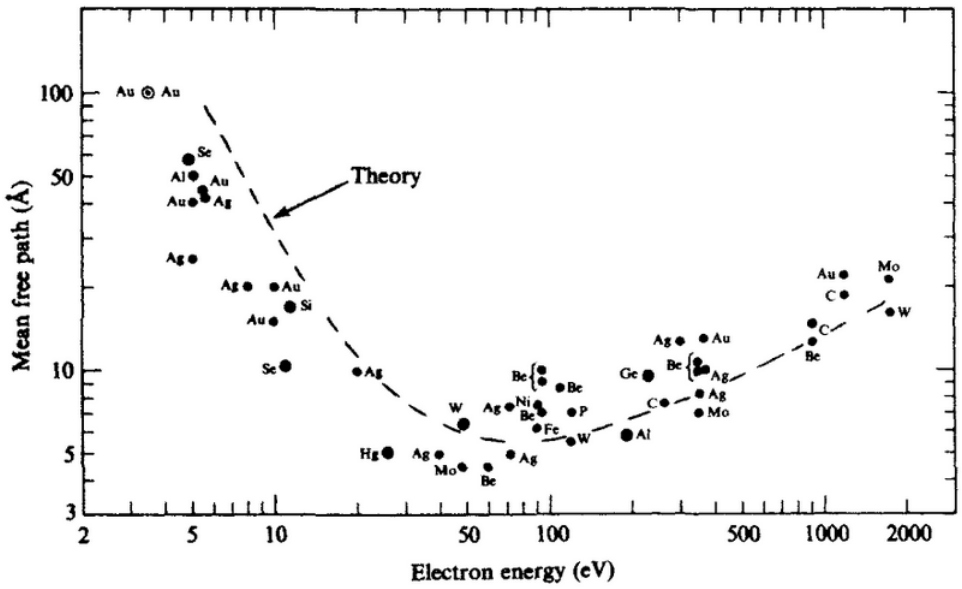

Figure 3.5: Universal curve of inelastic mean free path. Figure taken from [20].

The surface sensitivity of electrons can be illustrated with a plot of inelastic mean free path versus electron kinetic energy, where the data points scatter around a universal curve [20]. This is illustrated in figure 3.5. The inelastic mean free path (IMFP or λ) of an electron travelling within a solid can be defined as the mean distance it traverses before undergoing an inelastic event, i.e. some interaction whereby it loses energy [19]. The mean free path of the electrons in a sample will determine the surface sensitivity of the technique. The sampling depth of XPS is often defined as three times the IMFP (λ), the depth from which 95 % of the photoemission has taken place. Most of the λ values are in the range 1-3.5 nm for Al Kα-radiation, so the sampling depth under these conditions is 3-10 nm. From this it is given that XPS is an extremely surface sensitive technique.

3.1.2 Data analysis

A big advantage with XPS is that it is easy to obtain quantitative data, by determining the area under the peaks in question [19]. The intensity of a peak in the XPS spectrum is given by

$$I = Kn\sigma\lambda, \tag{3.3}$$

where K includes all the factors related to quantitative detection of a signal, and is assumed to remain constant during the measurements. n is the average atomic concentration of the element in question in the surface, σ is the photoelectron cross section for the element, and λ is the inelastic mean free path of a photoelectron in the element.

Estimating the relative amounts of elements in a sample, the sensitivity factor SF has to be known, along with the measured intensity of the element of interest. The theoretical sensitivity factor for the different elements can be retrieved from tables. Using this, we have that the corrected intensity is given by

$$I = \frac{A}{SF \cdot N}, \tag{3.4}$$

where A is the measured area under the peak, SF is the sensitivity factor, and N is the number of measurement iterations.

When doing experiments involving evaporation of a material on a surface, it is necessary to estimate the thickness of the evaporated layer. Assuming that the evaporated layer forms a thin film on the sample surface, a schematic is illustrated in figure 3.6. The thickness of the layer is given by a.

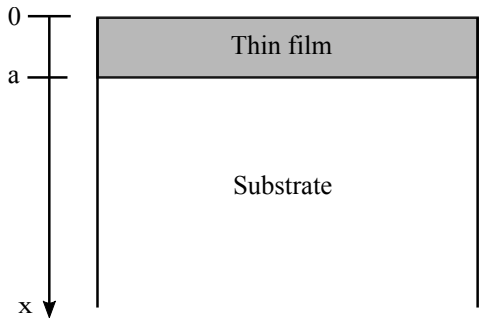

Figure 3.6: Schematic of thin film on a substrate.

The intensity of the thin film is given by

$$\begin{aligned} I_{\text{film}} &\sim \int_0^a e^{-\frac{x}{\lambda_{\text{film}}}} dx \\ &= \lambda_{\text{film}} \left(1 - e^{-\frac{a}{\lambda_{\text{film}}}}\right). \end{aligned} \tag{3.5}$$

In the same way, we find that the intensity of a chosen element in the substrate is given by

$$\begin{aligned} I_{\text{sub}} &\sim n_{\text{sub}} \int_a^\infty e^{-\frac{x}{\lambda_{\text{sub}}}} dx \\ &= n_{\text{sub}} \lambda_{\text{sub}} e^{-\frac{a}{\lambda_{\text{sub}}}}, \end{aligned} \tag{3.6}$$

where a is the thickness of the layer, λ is the inelastic mean free path of the element in the substrate or the layer, and n_{sub} is the assumed concentration of the element in the substrate. Dividing equation (3.5) with equation (3.6), we obtain

$$\begin{aligned} \frac{I_{\text{film}}}{I_{\text{sub}}} &= \frac{\lambda_{\text{film}} \left(1 - e^{-\frac{a}{\lambda_{\text{film}}}}\right)}{n_{\text{sub}} \lambda_{\text{sub}} e^{-\frac{a}{\lambda_{\text{sub}}}}} \\ &= \frac{\lambda_{\text{film}}}{n_{\text{sub}} \cdot \lambda_{\text{sub}}} \left(e^{\frac{a}{\lambda_{\text{sub}}}} - e^{-a\left(\frac{1}{\lambda_{\text{film}}} - \frac{1}{\lambda_{\text{sub}}}\right)} \right). \end{aligned} \tag{3.7}$$

For notational simplicity, we introduce $I_{\text{film}}/I_{\text{sub}} = I$, $\lambda_{\text{film}}/n_{\text{sub}} \cdot \lambda_{\text{sub}} = \gamma$, $1/\lambda_{\text{sub}} = \alpha$ and $(1/\lambda_{\text{film}} - 1/\lambda_{\text{sub}}) = -\beta$, which gives

$$I = \gamma \left(e^{\alpha a} - e^{\beta a} \right).$$

By equating

$$f(a) = I + \gamma e^{\beta a} \quad \text{and} \quad g(a) = \gamma e^{\alpha a}, \tag{3.8}$$

we can numerically find the thickness a of the thin film.

Before measuring the areas under the peaks in the XPS spectrum, a background is removed. In this work, the Shirley background has been used, which assumes that the background arises solely from inelastic scattering of electrons of higher kinetic energy. The background increases with increasing binding energy, forming an S-shaped background [8].

A model for morphological changes as a result of sample heating

Previous work has shown that nickel deposited on muscovite mica surfaces will change morphology if deposited at low temperatures and subsequently being heated to temperatures around 710 K. It is assumed that the nickel, when first deposited, covers the mica surface as a thin film, as illustrated in figure 3.6. After the sample is heated once, it is assumed that the nickel moves on the surface, forming clusters with a height twice the height of the thin film, covering only half of the mica surface. This is illustrated in figure 3.7.

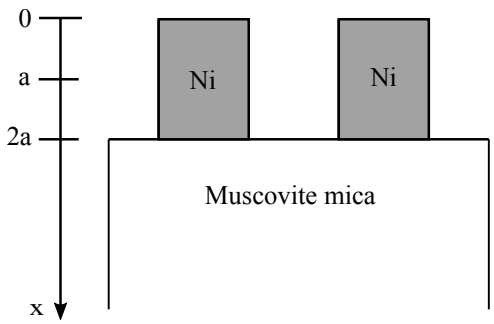

Figure 3.7: Schematic of nickel clusters on muscovite mica.

The intensity of the nickel can then be estimated by

$$\begin{aligned} I_{\mathrm{Ni}} &\sim \frac{1}{2}\int_0^{2a} e^{-\frac{x}{\lambda_{\mathrm{Ni}}}}\,dx \\ &= \frac{1}{2}\lambda_{\mathrm{Ni}}\left(1 - e^{-\frac{2a}{\lambda_{\mathrm{Ni}}}}\right), \end{aligned} \tag{3.9}$$

and the intensity of the mica surface can be estimated by

$$\begin{aligned} I_{\mathrm{mica}} &\sim n_{\mathrm{K}}\left(\frac{1}{2}\int_0^{\infty} e^{-\frac{x}{\lambda_{\mathrm{K}}}}\,dx + \frac{1}{2}\int_{2a}^{\infty} e^{-\frac{x}{\lambda_{\mathrm{K}}}}\,dx\right) \\ &= n_{\mathrm{K}}\frac{1}{2}\lambda_{\mathrm{K}}\left(1 + e^{-\frac{2a}{\lambda_{\mathrm{K}}}}\right). \end{aligned} \tag{3.10}$$

Calculating the relationship between the nickel and muscovite mica intensities both before and after heating, and plotting these as a function of the thickness of the initial thin film, it is clear that the difference between the relationships should be a lot bigger for the large nickel doses. This is illustrated in figure 3.8.

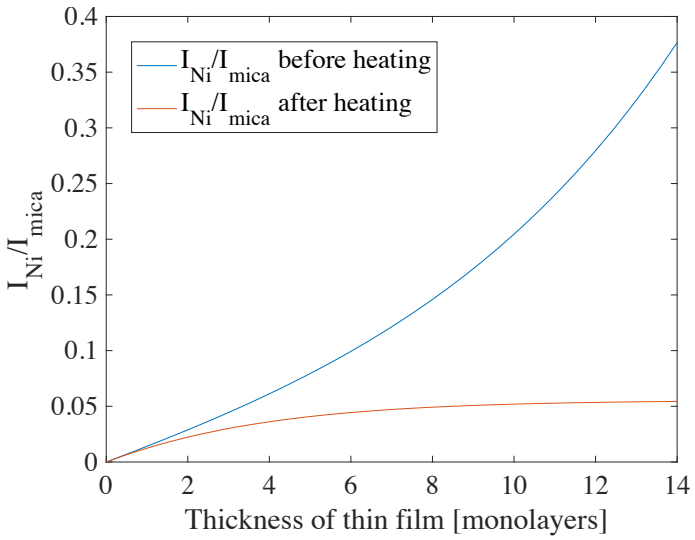

Figure 3.8: Relationship between the intensities of nickel and mica, before and after heating. The model indicates that with a thick initial nickel film, the estimated amount of nickel on the sample will be much smaller after heating. The change will not be as for the small nickel doses.

3.1.3 Instrumentation

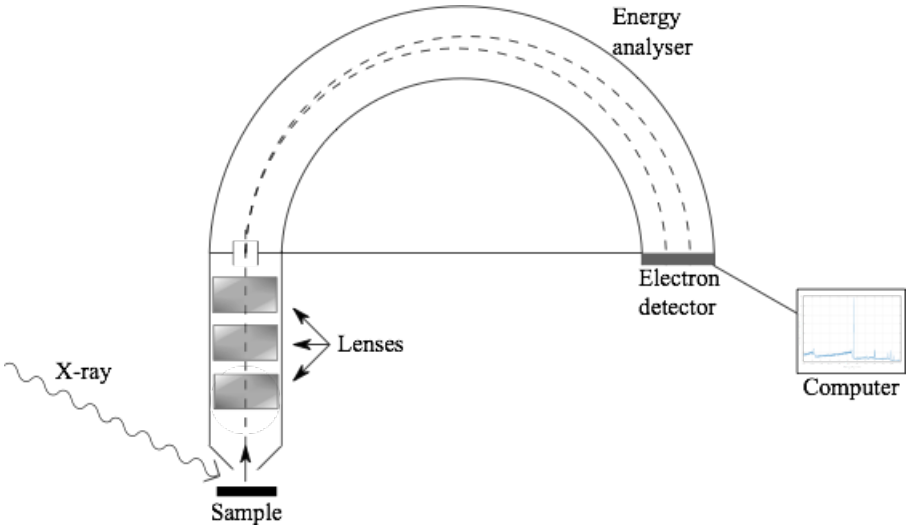

Figure 3.9: Schematic view of the XPS setup. The sample is irradiated with X-rays and emits photoelectrons. The photoelectrons are analysed and detected, before the result is presented in a graph.

The experimental setup consists of an X-ray source, a sample in an ultra high vacuum system, a set of electron lenses, an electron energy analyser and detector, and a computer system. Figure 3.9 shows a schematic view of the setup used.

A Scienta SES2002 spectrometer in conjunction with a monochromatised X-ray source (Al Kα) is used in this work. The X-ray source irradiates the sample with a photon energy of $h\nu = 1486.6$ eV. The photoelectrons emerging from the sample are sent through a lens system which focuses them onto the entrance of the energy analyser [18]. The electron energy analyser used is a concentric hemispherical analyser. The analyser performs energy dispersion of the incoming electrons by applying a voltage difference between the two concentric hemispheres. The centre line potential is known as the pass energy, which determines the energy resolution of the analyser and is held constant during the measurements. In these experiments, the pass energy is $E_{\text{pass}} = 200$ eV for the core-level scans and $E_{\text{pass}} = 500$ eV for the survey scans, which gives an energy resolution of about 0.4 and 1.0 eV, respectively. At the end of the analyser, the photoelectrons hit the detector, where they are counted before being presented in a graph on a computer.

In addition to the components described above, a low energy electron flood gun can be used to neutralise the surface charge build up on the material. The surface charge is due to the material's inability to replace photoemitted electrons. Muscovite mica is an insulating material which often develops a static surface charge when being irradiated by X-rays [19]. By manually tuning the flood gun, the right amount of current can be chosen, so that the peaks in the XPS scan are shifted back to their uncharged binding energies. In this work, an electron flood gun with energy 1 keV and current 2.2 A is used to compensate for the surface charge on the muscovite mica sample.

3.2 Temperature programmed desorption (TPD)

Thermal desorption from a surface is one of the simplest qualitative and quantitative experiments that can be carried out on a surface containing an adsorbed layer [21]. Temperature programmed desorption is, in general, a measure of the rate of desorption of adsorbed molecules as a function of temperature. The aim of the technique is to obtain an understanding of the nature of the adsorbate-substrate bonding [22].

3.2.1 Basic principles

A sample is heated with a temperature program $\beta(t) = dT/dt$ and the partial pressure of atoms and molecules desorbing from the sample is measured by mass spectrometry. As the temperature of the surface increases, the rate of evolution of gas increases as well, resulting in a rise of the instantaneous gas density. This happens at characteristic temperatures for different atoms and molecules, and gives a desorption peak in the TPD spectra at the characteristic temperature.

The rate of evolution from the surface of area A can be represented by an Arrhenius expression, known as the Polyani-Wigner equation [22],

$$r_{\mathrm{d}} = -\frac{d\theta}{dt} = \nu(\theta)\theta^n e^{-E_{\mathrm{d}}(\theta)/kT}, \tag{3.11}$$

where θ is the coverage of the adsorbate, $\nu(\theta)$ is the pre-exponential factor, $E_{\mathrm{d}}(\theta)$ is the activation energy for desorption, k is the Boltzmann constant, T is the temperature, and n is the order of desorption. The order of desorption is expected to be 0, 1 or 2 in thermal desorption. A zero order desorption is seen in multilayer desorption, first order occurs when a molecule adsorbs and then desorbs without dissociation, while in second order the molecule is dissociated on the sample before recombination and desorption. The second order curve is shifted towards lower temperatures, as the initial concentration is increased, while the first order desorption curve is independent of initial concentration.

Combining equation (3.11) and the equation for pressure rise ΔP in a vacuum chamber of volume V [21],

$$\frac{d(\Delta P)}{dt} = \frac{kT}{V}\left(-A\frac{d\theta}{dt}\right) - \frac{\Delta P}{\tau}, \tag{3.12}$$

the desorption rate can be expressed as

$$r_{\mathrm{d}} = \frac{V}{AkT}\left(\frac{d(\Delta P)}{dt}\right) + \frac{\Delta P}{\tau}. \tag{3.13}$$

Here, $\tau = V/S$ is the characteristic pumping time of the system, as S is the pumping speed, and the other parameters are explained above. If the pumping time τ is small enough, the desorption rate will be proportional to the change in ΔP ($r_{\mathrm{d}} \propto \Delta P/\tau$).

3.2.2 Data analysis

Figure 3.10 shows the desorption of 2.0 L[1], 1.0 L, 0.5 L and 0.1 L carbon monoxide from a nickel-decorated mica surface. The figure also shows how the kinetic parameters are estimated using the Polyani-Wigner equation and assuming first order desorption. Only the leading edge is fitted and used for the calculations, as illustrated by the curves under the first desorption peak in the TPD spectra in the figure.

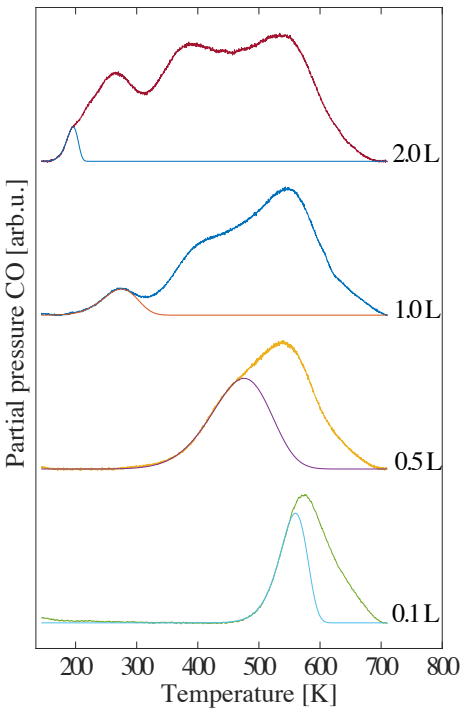

Figure 3.10: TPD spectra where the leading edges have been fitted to a first order desorption spectrum in order to extract an estimate of desorption parameters.

The thermal desorption spectra depend on several parameters, including the nature of the adsorption sites, molecular interactions on the surface, molecular orientation, surface diffusion, and dissociation and bonding at the sur-

[1][L] = Langmuir. 1 langmuir equals the gas exposure of 10^{-6} torr during one second [22].

face. By analysing the TPD scans, two main classes of information can be found [23]. First, the area under the TPD profile, which is proportional to the amount of adsorbate originally adsorbed. Second, the position of the peak maximum, which is related to the desorption energy $E_{\mathrm{d}}(\theta)$ and the pre-exponential factor $\nu(\theta)$. The pre-exponential factor is an indication of the degree of rotational and transitional freedom for the desorbed molecule. For a molecule in its ground state, the pre-exponential factor is in the order of 10^{13} s^{-1} for a first order process and in the order of 10^{-2} $\mathrm{cm}^2\mathrm{s}^{-1}$ for a second order process, but this can also change with the coverage.

It is usually more than one binding state for the adsorbate molecules on a surface, giving different desorption peaks in the TPD spectrum, as for the TPD spectra in figure 3.10. Low adsorption temperatures allow the binding of adsorbates with all active sites present in the structure, and often leads to complex TPD spectra. The higher the temperature of the peak maximum, the more difficult desorption, so this is a natural indication of a strong interaction between the adsorbate species and the active sites on the surface.

3.2.3 Instrumentation

The experimental setup in the TPD experiment is illustrated in figure 3.11a. The sample is placed in an ultra high vacuum chamber, connected to a system for temperature control. It is placed in front of a differentially pumped Prisma quadropole mass spectrometer (QMS) which measures the pressure rise [24]. The QMS is surrounded by a shield to minimise the effect of desorption from the vacuum chamber walls or gas interactions with the walls. The desorbed gas from the sample is ionised through electron bombardment before being accelerated by an electric field into a space between four rod-shaped electrodes. These electrodes are illustrated in figure 3.11b.

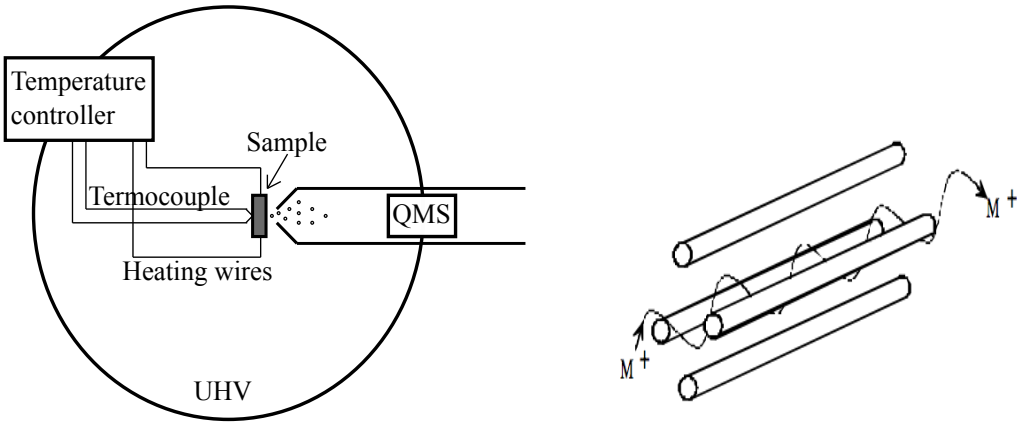

(a) The experimental setup of TPD

(b) The rod-shaped electrodes in a quadropole mass spectrometer

Figure 3.11: (a) Experimental setup, figure adapted from [23]. (b) Sketch of the four rod-shaped electrodes in the quadropole mass spectrometer, with the path of ions travelling between them. Figure (b) taken from [24].

In this space, the ions are separated according to their mass/charge-ratio (m/z), so that only chosen m/z-value ions can strike the detector. This m/z-value is determined by the radio frequency (RF) and the direct current (DC) voltages applied to the electrodes. The voltages produce an oscillating electric field that functions as a bandpass filter to transmit the selected m/z-values. At the end of the quadropole mass spectrometer, the detector measures the flux of ions at each m/z-ratio.

3.3 Atomic force microscopy (AFM)

Atomic force microscopy (AFM) is a method that allows for imaging and measurements of a surface structure in three dimensions with high resolution and accuracy, down to the nanometer scale [25]. The technique can be used to image almost any sample, both soft and hard, and it can be used in vacuum, air and liquid, making it an essential tool for materials and biological research. The atomic force microscope differs from other microscopes as it does not use light or electrons to form an image, but it physically feels the surface with a sharp probe and builds up a map of the height of the sample surface. In this work, the MultiMode V microscope at NTNU nanolab is used to image the topography of the nickel-decorated mica surfaces.

3.3.1 Basic principles

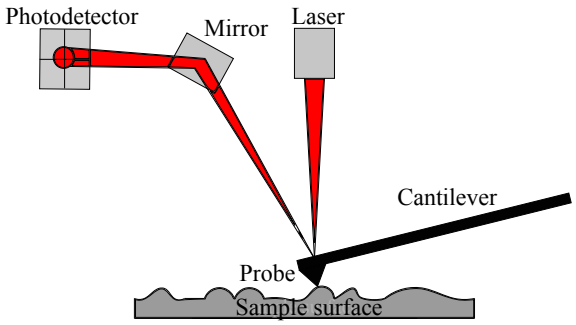

Figure 3.12: The basic principle of AFM, illustrating the main components of the technique. Figure adapted from [26].

The atomic force microscope touches the surface with a sharp probe, moves it laterally across the surface, and measures the vertical probe movement as the cantilever bends up and down to give height [26]. The experimental setup with the main components is illustrated in figure 3.12. A sharp tip is attached to a flexible cantilever which bends under the influence of force. This bending is measured by reflecting a laser beam off the cantilever and onto a split photodiode, which gives the deflection of the laser beam. The measured signal is used to control the movement of a piezoelectric device on which the cantilever is mounted. This feedback system makes the AFM a highly sensitive technique. By moving the probe over a two dimensional grid of locations on the sample, a surface topography can be imaged as height versus lateral position.

3.3.2 AFM modes

There are many different modes in which the atomic force microscope can be operated, the most common ones being topographic modes measuring the height of the sample surface as described above [25]. A variety of topographic modes have been developed, the main three being contact mode, non-contact mode, and tapping mode. In contact mode, the static deflection of the AFM cantilever is measured, while in non-contact and tapping mode, the dynamic oscillation of the cantilever is measured. Figure 3.13 shows a force-distance curve, illustrating in which regimes the three modes operate. The curve is calculated from a deflection-distance curve which is measured by monitoring the deflection of the cantilever as a piezo is used to move the tip towards the sample. At a set deflection level, the direction is typically reversed and the tip withdraws from the sample.

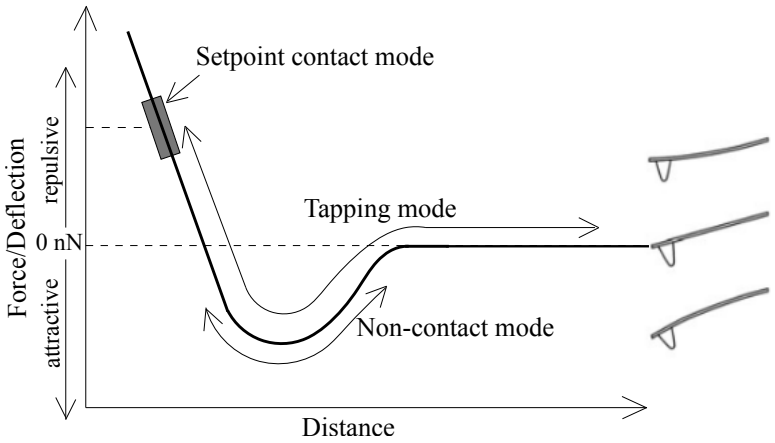

Figure 3.13: Force-distance curve illustrating in which regimes contact, non-contact and tapping mode, operate. The deflection of the cantilever is illustrated to the right in the figure. The figure is adapted from [25].

The cantilever is considered to have zero deflection when the tip is far from the sample surface, and as the tip approaches the surface, it feels an attractive force with a following snap-in as the tip becomes unstable and jumps into contact with the surface. As the instrument continues to push the cantilever towards the surface, the interaction moves into the repulsive regime, as shown in figure 3.13. In this regime, a combination of cantilever bending and sample compression occurs. Reversing the direction of the movement, the interaction passes again into the attractive regime, and the tip stays on the surface until instability occurs again, and the tip snaps off the surface.

Contact mode

Contact mode was the basis for the development of the later modes in AFM [25]. The mode operates in the repulsive regime, as illustrated by the grey box in figure 3.13. Only the static deflection of the AFM cantilever is measured in contact mode, making it the fastest of the topographic modes. The deflection signal is used with the feedback parameters to determine how the z piezo must move to maintain a constant cantilever deflection and constant tip-sample force. The amount the z piezo moves to maintain the deflection is taken to be the sample topography. This signal plotted versus distance, forms the height or topography image in contact mode.

The best reason to use contact mode is its high resolution, but the applied normal force leads to a high lateral force applied to the sample as well. For soft and weakly adsorbed samples, this can lead to problems of sample distortion, damage or even removal from the substrate.

Non-contact mode

The non-contact mode is an oscillating AFM mode, operating in the attractive regime. A generated oscillating signal is applied to the cantilever mechanically, making the probe oscillate close to its resonant frequency. When the oscillating probe approaches the sample surface, the oscillation changes due to the interaction between the probe and the force field from the sample. This again causes a monitored damping of the cantilever oscillation, and the feedback loop maintains the probe-sample interaction constant. In this mode, the frequency shift is used to image the surface topography.

This mode can have an advantage because of the low probe tip-sample forces that are involved in the imaging process.

Tapping mode

Tapping mode is another type of oscillating AFM mode, which operates in both the repulsive and the attractive regime. If a large oscillation is applied, the probe will move from being far from the surface where there is no tip-sample interaction, through the attractive regime, into the repulsive regime, and back, in each oscillation cycle. The feedback in tapping mode is usually based on amplitude modulation, and this amplitude signal can be used as an illustration of the shape of the sample.

Because of the large tip-sample forces involved in this mode, it can be more destructive than non-contact mode. However, it is much easier to implement, and the problematic lateral forces in contact mode do not affect

tapping mode. This is because the movement of the tip relative to the surface is perpendicular in the scanning process.

Peak force tapping mode

In this work, the peak force tapping mode is used, which is Bruker's own mode [27]. The probe periodically taps the sample and the small interaction force is measured directly by the deflection of the cantilever. This mode operates similarly to tapping mode in the sense that it avoids lateral forces by hitting the sample perpendicularly. However, the oscillation of the cantilever is at frequencies well below its resonant frequency. During the approach of the tip to the sample surface, the cantilever begins at a non-contact force at a discrete distance above the sample [28]. The z piezo pushes it downward until it touches the surface, then continues to gently push until the cantilever reaches a setpoint. The setpoint is a measure of the magnitude of the tip-sample interaction and is used to create the topography image. The z piezo then withdraws the tip from the surface, making it return to its original non contact force.

3.4 Ultra high vacuum (UHV)

For XPS and TPD, ultra high vacuum conditions are required, which means that the pressure has to be smaller than about 10^{-9} mbar ($\sim 10^{-9}$ torr) [8].

Under the conditions of 1 atm (= 760 torr), there are more than 10^{23} collisions/cm$^2\cdot$ s. Looking at e.g. a silicon surface, a contaminant monolayer will form within a few nanoseconds at room temperature under this pressure. This time interval will increase to about 1000 s when the pressure is 10^{-9} torr. Under atmospheric conditions, there are also roughly $2 \cdot 10^{19}$ molecules/cm^3. Such a density will prohibit the photoelectrons from travelling undisturbed from the sample to the detector, and the X-rays from travelling from their source to the sample in XPS.

Achieving ultra high vacuum is accomplished by reducing the amount of molecules in the chamber, which is done with a specialised pumping system, consisting of e.g. turbomolecular and ion pumps, and a chamber with very low outgassing characteristics.

Turbomolecular pump

The turbomolecular pump consists of a series of bladed turbine rotors on a shaft that rotates with 20 000 to 90 000 rpm [29]. The rotor blades are canted so that when a molecule strikes a blade it receives momentum in the

direction of the pump exhaust. Stationary blades are interleaved between the rotors, and are canted in the opposite direction from that of the rotors to decelerate the molecules and compress the flowing gas before it is sent towards the next rotor-stator pair. Most gases can be pumped with this system, although they do not efficiently pump hydrogen and helium.

Ion pump

An ion pump consists of a stainless steel anode and a titanium cathode, with an electric field between them [29]. This electric field ionises inert-gas molecules and other molecules, accelerating them towards the cathode, which buries them permanently. Active gases are chemisorbed by titanium that has been sputtered off the cathode by ion bombardment and deposited on the anode. The ion pumps function between 10^{-2} and 10^{-11} torr, but has a limited lifetime when being used above 10^{-5} torr, so a forepump is used to reach the starting pressure.

3.5 Sample preparation

The muscovite mica substrate used in the experiments are obtained from Goodfellow Cambridge Ltd., England. The samples are of best quality, grade 5, and they are circular with a diameter of 12 mm and a thickness of 0.15 mm.

A freshly cleaved mica surface is expected to be covered with potassium ions that are not in a specific structure [9]. These ions are assumed to react strongly with part of the surrounding atmosphere, giving a contaminant layer containing mainly carbon. It has therefore been important to have a good procedure for cleaning the samples.

3.5.1 Scotch tape cleaving

Before the sample is placed in the vacuum chamber, it is cleaved with scotch tape in air. Some of the samples are also cleaved in vacuum ($P \sim 10^{-7}$ torr), when moving the sample from the load lock to the preparation chamber. Figure 3.14 shows how the sample is installed with tape in the load lock. One end of the tape is attached to the surface of the sample, while the other end is attached to the wall of the load lock. In this way the sample is cleaved, as the tape remains attached to the wall, when being moved from the load lock to the preparation chamber.

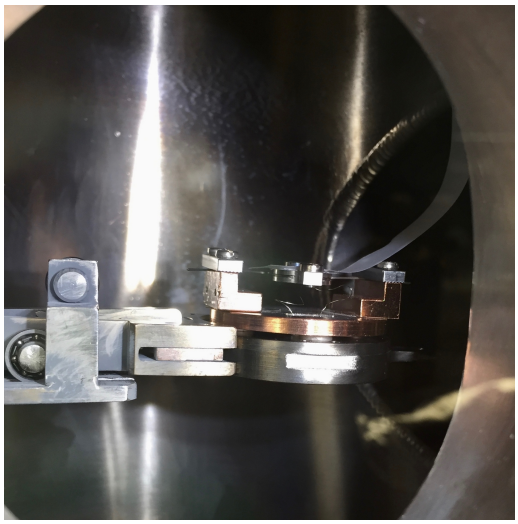

Figure 3.14: The sample is installed in the load lock with scotch tape attached to its surface for cleaving in vacuum.

The scotch tape method is not always perfect, as it is difficult to assure that the contaminant layer has been removed. This is especially a problem for the scotch tape cleaving in vacuum, so this part of the preparation has been skipped in some of the experimental runs. Other methods for surface cleaning have always been performed after the scotch tape cleaving to ensure a clean surface.

3.5.2 Thermal treatment

This experiment depends on the sample having temperatures in the range of $120 - 750$ K. A proportional-integral-derivative (PID) controller was used to control the temperature of the sample during the different parts of the experiments.

After the sample is placed in the preparation chamber, it has to be degassed to remove any gases from the surface. This is achieved by heating the sample up to 700 K until the pressure was stable at this temperature. It is known that untreated mica has a fairly high concentration of water incorporated into its bulk, and that this water can play an important role in metal particle nucleation and growth [10]. Because of this, the samples are annealed over night at 700 K before conducting the experiments, to get rid of as much water as possible.

In the deposition of nickel, evaporation of CO, and the TPD experiments, the samples were cooled down to temperatures well below room temperature. This was achieved with liquid nitrogen.

3.5.3 Hydrogen atom bombardment

An effective method for surface cleaning is hydrogen atom bombardment. It is a chemical method for cleaning which is effective without being too aggressive to the surface, removing the most common contaminants, including carbon [30]. The technique used in this experiment was invented by Langmuir in the early 1900s [31]. The experimental setup is presented in figure 3.15. Hydrogen gas is introduced into the preparation chamber, at a pressure of $2 \cdot 10^{-6}$ torr and a temperature of 700 K. Inside the chamber, a tungsten filament is placed close to the sample, and heated with a current of 1.5 A. When the filament is heated, the H_2 molecules hitting it are dissociated and hydrogen atoms are accelerated away from the filament.

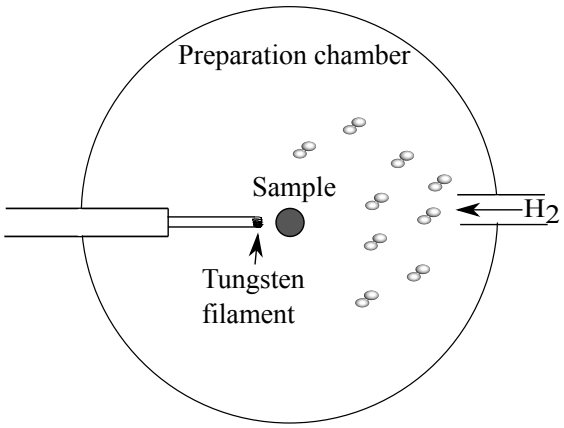

Figure 3.15: Schematic view of the experimental setup in hydrogen atom bombardment.

Sugaya & Kawabe studied this technique for cleaning GaAs substrates, looking at two possibilities for what happens at the surface when being hit by hydrogen atoms [32]. One possibility is physical sputtering, where incident hydrogen atoms impact with high energy on the surface. This energy is transferred to the carbon atoms at the surface, and when it is sufficient to overcome the surface binding energy, the carbon atoms will escape from the surface. Since the energy of the incident atomic hydrogen generated by a tungsten filament is too low, physical sputtering contributes minimally to the cleaning process. The other possibility is that a chemical reaction takes place, and this is assumed to be the main cleaning mechanism. Active atomic hydrogen combines with atomic carbon at the surface by a chemical reaction, forming hydrocarbon which escapes to the surrounding atmosphere.

This technique has some limitations. There is only a low probability that a molecule striking the filament will dissociate [31]. It is found that the sticking probability is temperature independent at temperatures above 2100

K, at a value of about 0.3. If the tungsten temperature is high enough, all molecules sticking to it are evaporated as atoms, and the 0.3 value represents the sticking probability for H_2 molecules incident on a tungsten surface. As a consequence, prolonged exposures are needed. In this work, the hydrogen treatment is performed for one hour, which we have found to be sufficient. XPS scans of a mica sample before and after a one hour hydrogen treatment is presented in figure 3.16a, showing how the carbon contamination on the surface is completely removed.

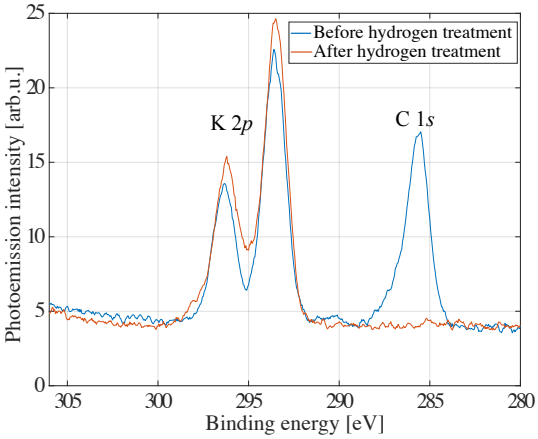

(a) XPS of mica before and after hydrogen atom bombardment

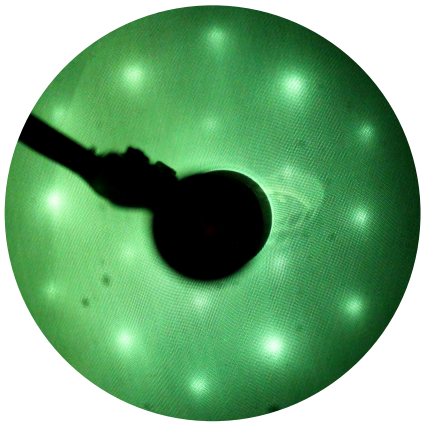

(b) LEED image of mica sample after annealing and hydrogen treatment

Figure 3.16: Figure (a) shows XPS scans before and after one hour hydrogen atom bombardment. Figure (b) shows a LEED image of the sample after annealing process and hydrogen treatment. LEED pattern is obtained at an electron energy of 112 eV.

To make sure that the sample surface was not disrupted by the annealing process and the hydrogen treatment, a low energy electron diffraction (LEED) image was taken of the sample. The LEED image is shown in figure 3.16b and it clearly illustrates the hexagonal atomic structure of the aluminosilicate layers in muscovite mica.

3.5.4 Evaporation of nickel

Evaporation of nickel onto the mica sample was done using two different methods, illustrated in figure 3.17. Thermal evaporation was done by heating a tungsten wire formed as a basket around a lump of nickel. Heating the tungsten wire heats up the nickel lump, and nickel atoms are evaporated towards the sample. The other method used was with an electron beam

evaporator. A nickel rod is installed inside an evaporator. Keeping the rod at high voltage, an electron current is drawn from a nearby hot filament and heats up the tip of the rod. When the tip is heated, nickel is evaporated towards the sample.

(a) Tungsten wire basket **(b)** E-beam evaporator

Figure 3.17: Figure (a) shows the tungsten wire basket [1]. Figure (b) shows the electron beam evaporator [2].

The amount of nickel evaporated on the sample is estimated using a quartz crystal oscillator evaporation monitor in both methods. Varying the current sent through the tungsten wire, and the electron current in the electron beam evaporator, the evaporation rate could be controlled. The evaporation rate is assumed to be 0.01-0.02 Å/s for the thermal evaporation when a current of 12 A was sent through the wire. For the electron beam evaporator, the evaporation rate was kept at either 0.015 Å/s or 0.03 Å/s. The evaporation was performed at a sample temperature of 150 K, and the base pressure varied around 10^{-9} torr for thermal evaporation and 10^{-10} torr for electron beam evaporation. After evaporation, the nickel amount on the mica surfaces was calculated from XPS measurements.

3.5.5 Adsorption of CO

Carbon monoxide (CO) is the most commonly studied adsorbate [33]. It is used as the adsorbate in this work to investigate the fundamentals of

[1]Taken from `https://www.lesker.com/newweb/evaporation_sources/thermal_basketheaters.cfm?pgid=1`

[2]Taken from `https://www.prevac.eu/en/2,offer/37,instruments/125,electron-beam-evaporator-ebv-40a1.html`

adsorption and desorption, and because catalytic reactions involving CO are important in a number of applications.

CO was let into the preparation chamber via a gas leak valve at sample temperature $T = 150$ K and chamber pressure $P = 1{\cdot}10^{-8}$ torr or $P = 1{\cdot}10^{-7}$ torr, depending on the amount of CO being introduced. The amount of CO introduced to the chamber is measured in langmuir [L], and the CO dose was varied between 0.05 L and 10 L.

4 Results

In this chapter, the main results will be presented, divided in the sections "XPS", "TPD" and "AFM". Some of the results will be discussed briefly after being presented in this chapter, while the main results will be further discussed in the next chapter. Some additional results from the TPD measurements are presented in Appendix A, along with some brief comments.

4.1 XPS

X-ray photoelectron spectroscopy is used mainly for characterisation of the muscovite mica samples. It is used to check that the samples are clean after cleaving, annealing and hydrogen treatment, and to make an estimate of the amount of nickel evaporated on the mica surface. XPS is also used to check for carbon leftovers on the samples after the CO adsorption and desorption cycles.

4.1.1 Characterisation of muscovite mica

The XPS result of a cleaned muscovite mica sample is shown in figure 4.1. The spectrum shows no carbon contamination on the surface, and only the expected elements for muscovite mica are present and identified in the spectrum.

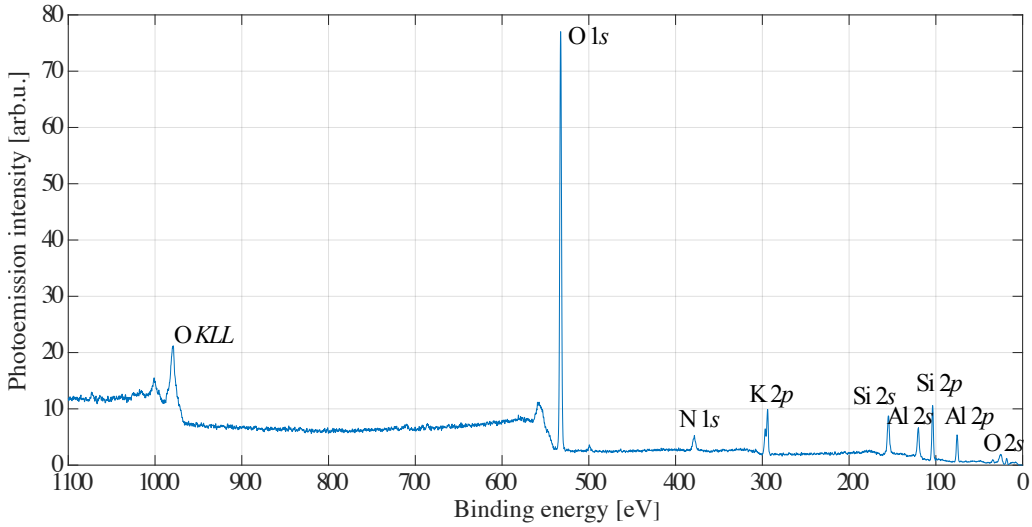

Figure 4.1: XPS survey spectrum of a clean muscovite mica surface. The different elements are identified in the spectrum.

4.1.2 Nickel-decorated muscovite mica

The estimated amounts of nickel on the mica surfaces are given in table 4.1. The estimates are obtained using the method described in section 3.1.2. To find the corrected intensities of the Ni $2p$ and K $2p$, sensitivity factors SF of 19.47 and 3.93, respectively, are used. The mean free path lengths λ used in the calculations are 18 Å for K and 10 Å for Ni. The amount n_{sub} of potassium in the mica sample is assumed to be 10 %.

Due to some problems with the experimental setup, XPS measurements were not always attainable. The "x" in the table marks where this was the case, and no XPS measurements were obtained. In these instances, the amount of nickel is assumed to be similar to another sample which is prepared with the same evaporation rate and time. E.g. sample nr. 9 is assumed to have approximately the same amount as samples nr. 7 and 8. When XPS measurements are only obtained either before or after heating, the amount is assumed to be a bit larger or smaller, depending on which results we have obtained.

Sample nr.	Ni amount before heating [ML]	Ni amount after heating [ML]
1	0.23	0.20
2	x	0.56
3	x	0.64
4	7.36	2.87
5	0.10	0.08
6	0.23	0.16
7	x	0.37
8	0.53	x
9	x	x
10	0.56	0.52
11	1.28	1.01
12	0.72	0.50
13	0.80	0.70
14	12.72	4.00

Table 4.1: The estimated amount of nickel evaporated on the mica surface, before and after heating of the sample. The estimates are given in [ML] = monolayers. Estimates are obtained using the method described in section 3.1.2. An "x" in the table implies that no XPS results are obtained because of problems with the setup.

From the estimated amount of nickel on the mica surface, and from looking at XPS spectra of samples before and after heating, it is clear that there

are morphological changes on the surfaces heated to temperatures around 710 K. Figure 4.2 shows the survey spectrum of sample nr. 4, both before and after heating. This sample was estimated to have approximately 7.4 monolayers of nickel on its surface before heating, and approximately 2.9 monolayers of nickel after heating. By just looking at the XPS spectra, it is clear that the nickel peaks are larger before heating and that the mica peaks are more visible after heating. The estimated amounts in table 4.1 show that the difference between the estimated nickel amounts is larger for the samples with a lot of nickel. It is assumed that this is due to a change from a thin film to clusters, as presented by a simple model in section 3.1.2. Figure 3.8 shows that according to this model, the change should be increased with increased nickel amount.

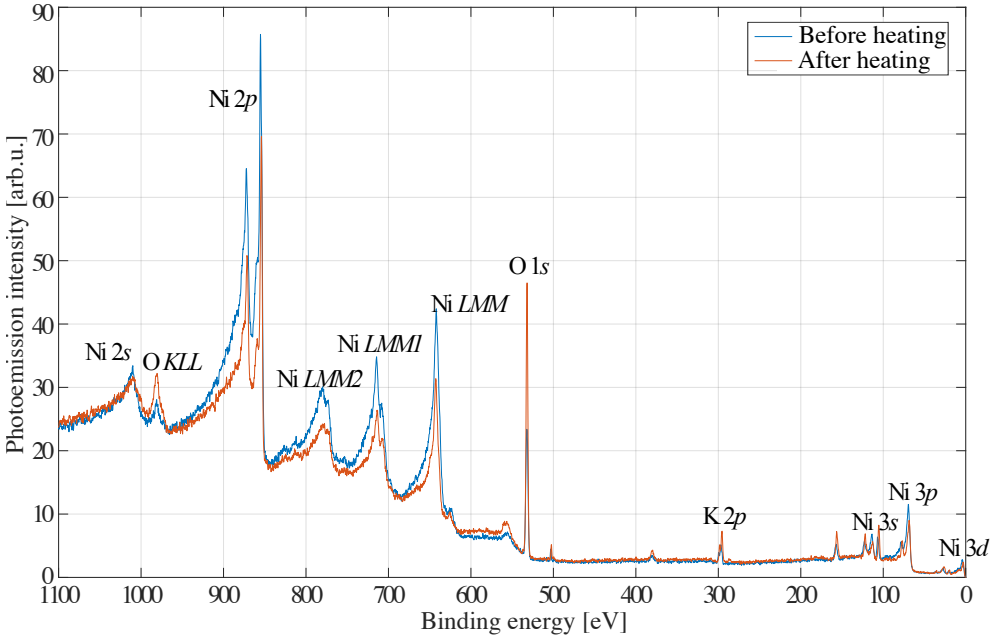

Figure 4.2: XPS survey spectrum of Ni-mica sample nr. 4, before and after heating. The sample was estimated to have approximately 7.4 monolayers of nickel on its surface before heating, and approximately 2.9 monolayers of nickel after heating.

4.1.3 Evidence of CO decomposition

Carbon monoxide can adsorb on the Ni-mica surface either as CO molecules or it can decompose to carbon and oxygen atoms. Some evidence is found for CO decomposition on our surfaces. Figure 4.3 illustrates the development of the carbon peak throughout the experiment for sample nr. 5, which has approximately 0.1 monolayers of nickel on its surface. The XPS measurements are performed after sample annealing and cleaning, after evaporation of nickel, and after a series of CO adsorption and desorption cycles. The sample showed no carbon before the CO adsorption, and since there was a small increase in the carbon peak after the adsorption and desorption, it is thought that this might be because of CO decomposition.

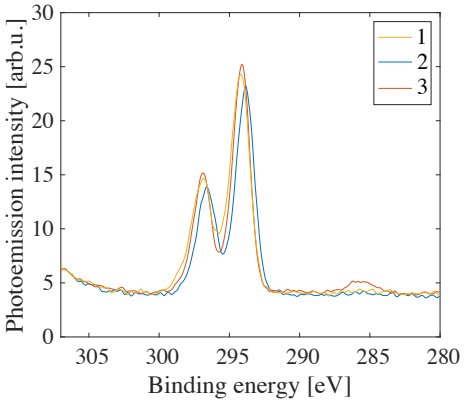

Figure 4.3: XPS spectrum showing the development of the K $2p$ (295 eV) and C $1s$ (285 eV) peaks during the experiment, for sample nr. 5 with approximately 0.1 monolayers of nickel. 1. XPS measurements after scotch tape cleaving, annealing process and hydrogen treatment. 2. XPS measurements after nickel evaporation. 3. XPS measurements after a series of CO adsorption and desorption cycles.

Almost all of our samples showed a small carbon peak after the TPD (CO adsorption and desorption) series. For some of the samples XPS measurements before CO adsorption are missing, making it impossible to know if the carbon is due to CO adsorption or simply leftovers from carbon contamination before the sample preparation. Also, some of the samples showed a small carbon peak before CO adsorption. It is therefore difficult to conclude concerning CO decomposition on different samples, but it is clear that some of the samples do not desorb all of the adsorbed carbon monoxide.

4.2 TPD

The temperature programmed desorption is focused on the adsorption and desorption of CO on the nickel-decorated mica samples. TPD series are done for samples with different doses of nickel, and for samples that are annealed at different temperatures, and prepared differently in terms of substrate temperature during nickel evaporation. In addition to the presented TPD spectra, kinetic parameters are found for most of the series. The kinetic parameters, desorption energy and pre-exponential factor, are obtained by fitting the leading desorption edge, as described in section 3.2.2.

The results that are considered to be most important are presented in this section, while some additional TPD results are presented in Appendix A. These additional results strengthen our conclusions, as they are similar to the results presented in this section.

4.2.1 Variation in nickel amount

The main part of this work has been to investigate how the adsorption and desorption vary with varying the amount of nickel deposited on the mica surfaces. Three different TPD spectra for CO desorption are observed, from a small, medium and large dose of nickel on mica. Results for four different samples are included in this section. Sample nr. 1 has a small amount of nickel on the surface, sample nr. 2 and 3 are considered having a medium amount of nickel, while sample nr. 4 has a large amount of nickel. Two medium amount samples have been included here to show that there is not found any significant difference between results obtained after thermal or electron beam evaporation of nickel. This also indicates that the evaporation rate is not that important in these results.

For the four samples presented here, both nickel and carbon monoxide were administered at a substrate temperature of 150 K. The samples were all cleaved, annealed at 700 K overnight, and hydrogen treated, prior to Ni and CO exposure.

Sample nr. 1

Sample nr. 1 is estimated to have approximately 0.23 monolayers of nickel on its surface before heating, which changes to 0.20 monolayers after heating. Figure 4.4 shows the TPD spectra of CO adsorbed on the surface, along with the kinetic parameters for the various CO exposures.

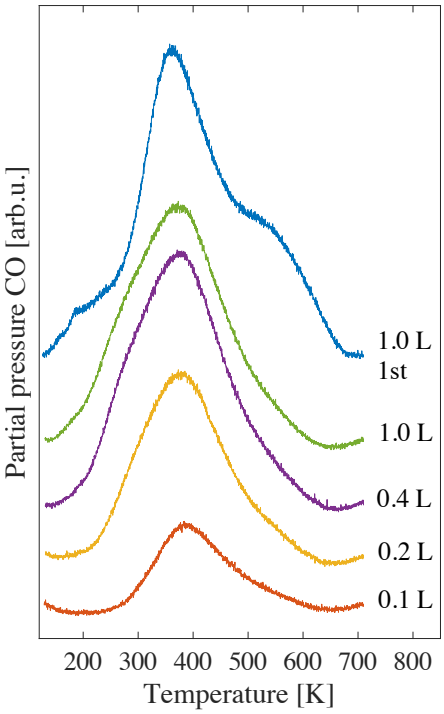

(a) TPD spectra from CO on Ni-mica

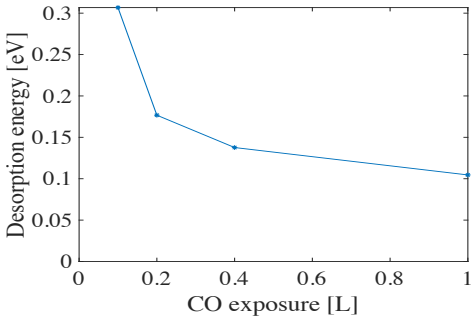

(b) Variation in desorption energy with coverage

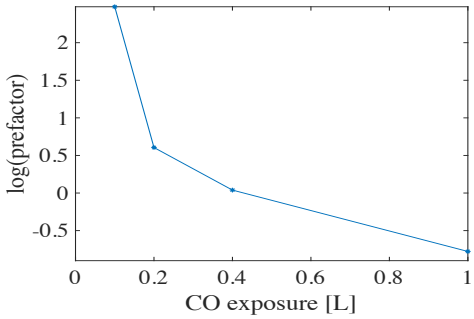

(c) Variation in prefactor with coverage

Figure 4.4: (a) TPD spectra of CO from 0.2 monolayers of nickel on mica. The CO exposure is given in the figure. Ni was deposited by thermal evaporation. The top spectrum represents the first run, and the other spectra are subsequent runs. The spectra are shifted vertically for clarity. Temperature ramp was 1 K/s. (b) and (c) Desorption energy and pre-exponential factor as a function of CO coverage.

The desorption energy is found to range from approximately 0.3 eV to 0.12 eV, where the smallest CO coverage gives the largest desorption energy. The corresponding pre-exponential factor ranges from $10^{2.5}$ to $10^{-0.8}$ s^{-1}. These numbers indicate that the CO does not have a strong bond to the Ni-mica surface, and that the desorption is not of first order.

For all CO coverages, there is a peak at around 390 K, and for coverages larger than 0.4 L, there is an extension towards 250 K. The TPD spectra also seem to have an extension towards 570 K.

It is clear that the CO adsorption changes from the first to the subsequent runs, as a result of morphological changes in the sample surface. The area under the 1.0 L desorption peak decreases with approximately 23 % from the first to the second run.

Sample nr. 2

Sample nr. 2 is estimated to have approximately 0.56 monolayers of nickel on its surface after heating, and the amount is assumed to be a bit larger before heating. Figure 4.5 shows the TPD spectra of different CO coverages on the Ni-mica surface, along with the kinetic parameters.

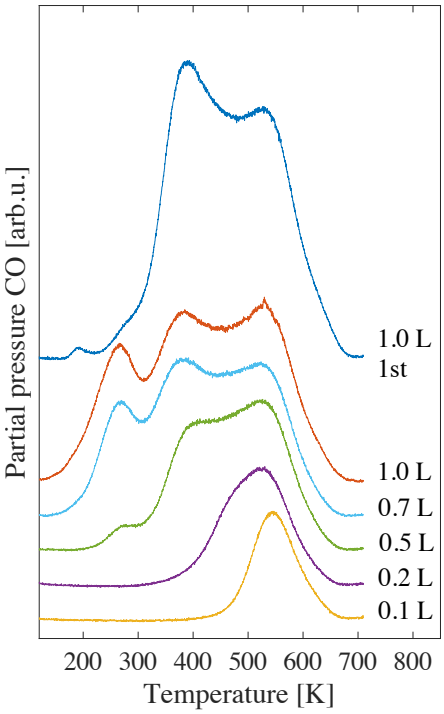

(a) TPD spectra from CO on Ni-mica

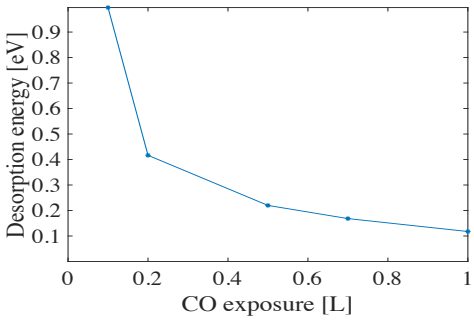

(b) Variation in desorption energy with coverage

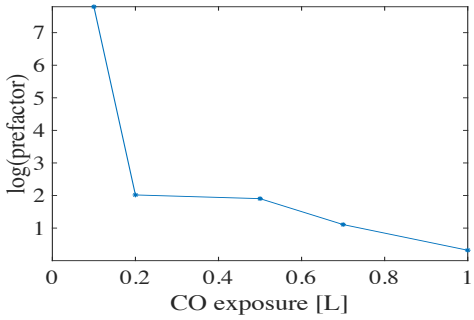

(c) Variation in prefactor with coverage

Figure 4.5: (a) TPD spectra of CO from 0.56 monolayers of nickel on mica. The CO exposure is given in the figure. Ni was deposited by thermal evaporation. The top spectrum represents the first run, and the other spectra are subsequent runs. Temperature ramp was 1 K/s. (b) and (c) Desorption energy and pre-exponential factor as a function of CO coverage.

The desorption energy ranges from 1.0 to 0.1 eV, with decreasing desorption energy for increasing CO coverage. The corresponding pre-exponential factor ranges from 10^8 to $10^{0.5}$ s^{-1}, indicating a desorption which is not of first order.

For all CO coverages, there is a desorption peak around 550 K, with an increasing peak at 380 K and 250 K for the larger CO coverages. This indicates that the adsorption sites with the strongest binding fill up first. The sites with strongest binding are the ones with a desorption energy around 1.0 eV, and the loosest bound are the ones with a desorption energy around 0.1 eV.

Also for this sample, the area under the 1.0 L CO desorption peak decreases with about 23 % from the first to the second run.

Sample nr. 3

Sample nr. 3 is estimated to have approximately 0.64 monolayers of nickel on its surface after heating. The amount is assumed to be a bit larger before heating. Figure 4.6 shows the TPD spectra for different CO coverages, along with the kinetic parameters.

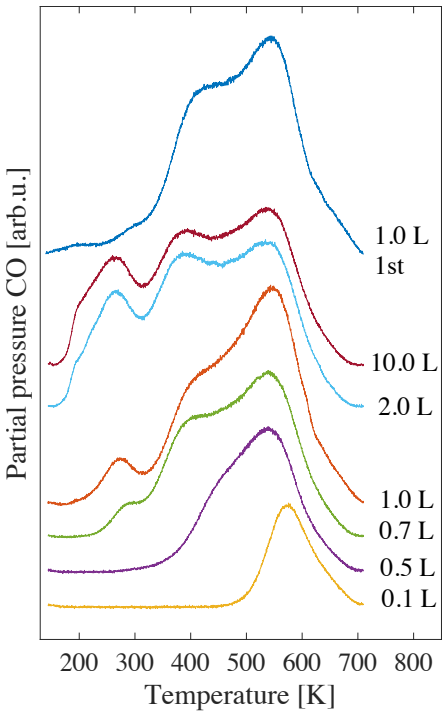

(a) TPD spectra from CO on Ni-mica

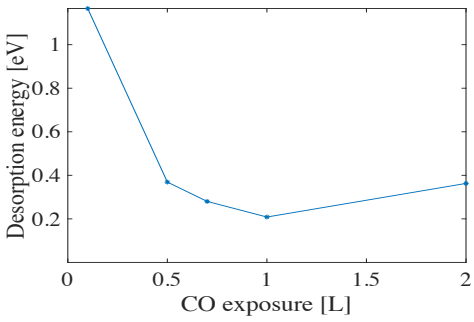

(b) Variation in desorption energy with coverage

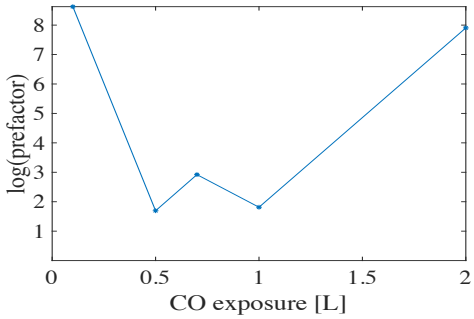

(c) Variation in prefactor with coverage

Figure 4.6: (a) TPD spectra of CO from 0.64 monolayers of nickel on mica. The CO exposure is given in the figure. Ni was deposited by electron beam evaporation. The top spectrum represents the first run, and the other spectra are subsequent runs. Temperature ramp was 1 K/s. (b) and (c) Desorption energy and pre-exponential factor as a function of CO coverage. The kinetic parameters for 10.0 L were approximately in the same range as for 2.0 L.

The desorption energy ranges from 1.2 to 0.2 eV, with the highest desorption energy for the smallest CO coverage. For 2.0 L and 10.0 L CO coverage, the desorption energy was found to be approximately 0.4 eV. The corresponding pre-exponential factor was found in the range $10^{8.5}$ to 10^{2} s^{-1}, indicating that there is not a first order desorption for these surfaces.

The desorption peaks are similar to the ones for sample nr. 2. All of the CO coverages have a desorption peak at 550 K, with increasing peaks at 400 K and 250 K with increasing CO coverage.

The change in area from the first to the second 1.0 L CO desorption spectrum was not as big as for sample nr. 1 and nr. 2, as the decrease was approximately 5 %.

Sample nr. 4

Sample nr. 4 is estimated to have approximately 7.4 monolayers of nickel on its surface before heating, and 2.9 monolayers after heating. Figure 4.7 shows the TPD spectra for the various CO coverages, along with the kinetic parameters.

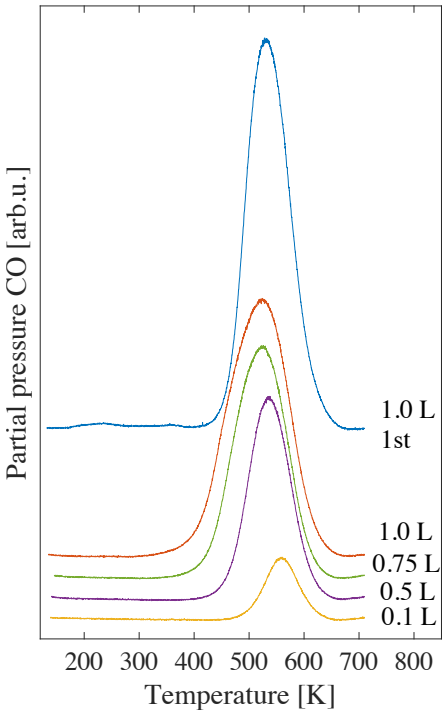

(a) TPD spectra from CO on Ni-mica

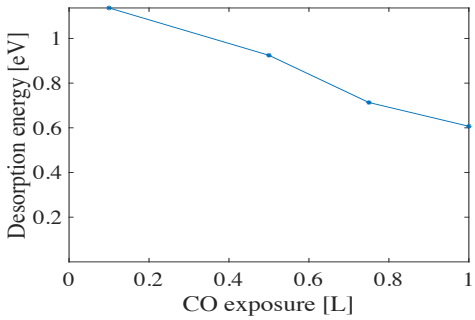

(b) Variation in desorption energy with coverage

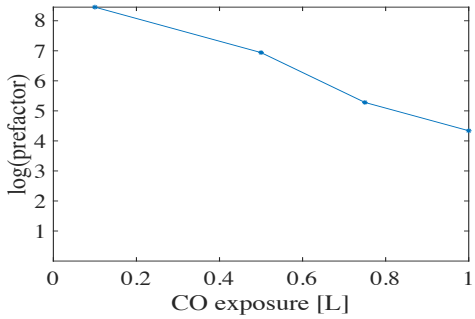

(c) Variation in prefactor with coverage

Figure 4.7: (a) TPD spectra of CO from 7.4/2.9 monolayers of nickel on mica. The CO exposure is given in the figure. Ni was deposited by electron beam evaporation. The top spectrum represents the first run, and the other spectra are subsequent runs. Temperature ramp was 1 K/s. (b) and (c) Desorption energy and pre-exponential factor as a function of CO coverage.

The desorption energy ranges from 1.2 to 0.65 eV, with the highest desorption energy for the smallest CO coverage. The corresponding pre-exponential

factor is found to range from $10^{8.5}$ to $10^{4.3}$ s^{-1}. This indicates that all of the CO binds quite strongly to this Ni-mica surface, as the desorption energy for all of the coverages are in the higher region. There is no first order desorption for this system either.

This surface only showed one peak in the TPD spectra, at around 550 K. The peak increases with CO coverage, but no additional peaks appear.

The reduction in adsorbed CO on the surface, from first to second 1.0 L CO exposure, is found to be about 10 %.

Summary of the results from varying the nickel amount

Three different desorption spectra are found by varying the amount of nickel on the mica surfaces, depending on having a small, medium or a large dose of nickel. The small doses range from 0.1 to 0.23 monolayers of nickel on the mica sample. These samples all have a main desorption peak at around 400 K, with an additional shoulder around 280 K for the larger CO coverages. An extension of the spectra towards 570 K is also observed for these samples. The medium doses range from 0.5 to 1.3 monolayers of nickel on their surfaces, having three distinct peaks in the TPD spectra, around 250 K, 400 K and 550 K. The main peak for these surfaces is the one at 550 K, with increasing peaks at 400 K and 250 K with increasing CO coverage. The large doses range from 2.9 to 4.0 (7.4 to 12.7 before heating) monolayers of nickel on the mica surface, and these samples only have one desorption peak at around 550 K.

All of the desorption spectra show a change in CO adsorption between the first and the second 1.0 L CO adsorption. This is evident from a decrease in the area under the desorption spectra from the first to the second run, and is a result of a change in surface morphology during the heating of the samples in TPD.

The desorption energies range from 0.1 to 1.2 eV, with the sample with a small nickel dose having only low desorption energies, the samples with the medium dose having desorption energies in the entire range, and the sample with the large dose having only the larger desorption energies. The estimates of desorption parameters assume first order desorption where a typical pre-exponential factor may be on the order of 10^{13} s^{-1}. The lower values observed may be indiciative of partially dissociative adsorption of CO on these samples. However, the analysis of the low temperature edge of the spectrum takes place in a regime where the coverage is slowly varying and a useful estimate of the desorption energy is obtained.

4.2.2 Variation in annealing procedure

Samples nr. 7, 8 and 9 are assumed to have approximately the same amount of nickel on their surfaces, being estimated to around 0.5 monolayers before heating. However, the annealing procedure is different for the three samples. Sample nr. 7 is only heated to 600 K for one hour prior to the nickel evaporation and the CO adsorption, sample nr. 8 is annealed at 600 K overnight, while sample nr. 9 has followed the normal procedure, being annealed at 700 K overnight. Figure 4.8 shows the TPD spectra for the second 1.0 L CO coverage for the different samples. The rest of the TPD results for the three samples are presented in Appendix A, in figures A.3, A.4, and A.5.

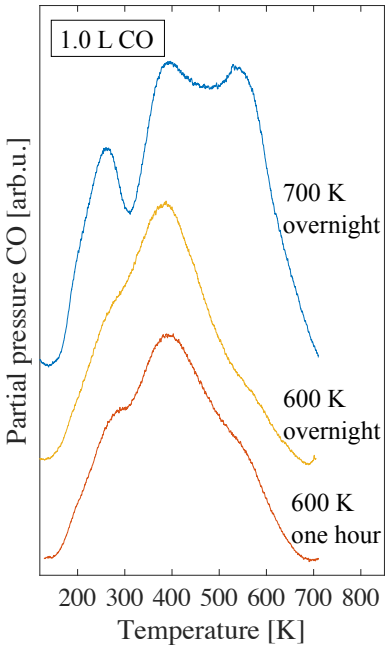

Figure 4.8: TPD spectra from the second 1.0 L CO coverage for three samples with different annealing procedures. All of the samples are assumed to have approximately 0.5 monolayers of nickel on their surface before heating.

For the initial desorption, the desorption energy was approximately the same for all 1.0 L CO coverages, around 0.2 eV. The difference seems to lie in the amount of CO adsorbed at the different adsorption sites, as the intensity of the peaks were quite different. The sample which was annealed at 700 K overnight had the most distinct peaks, the biggest difference being for the peaks around 280 K and 550 K, compared to the two other samples. The amount of CO adsorbed on the surface was smallest for the sample being annealed at 600 K for one hour, but the amount was not much larger for the

sample annealed at 600 K overnight. The amount of CO adsorbed on the sample annealed at 700 K overnight was almost 70 % larger than the two other samples.

The differences in the TPD spectra obtained from samples being annealed in different ways are assumed to be because of water in the bulk of the samples. It is known that an untreated mica sample has a fairly high concentration of water incorporated into its bulk, and that this water can play an important role in metal particle nucleation and growth [10]. Not knowing how the nickel is grown on the different samples, it is difficult to say exactly why the different samples adsorb CO differently. However, it is clear from the results that the sample annealed at 700 K overnight adsorbs the largest amount of CO.

4.2.3 Variation in nickel evaporation temperature

Samples nr. 2 and 10 were evaporated with the same amount of nickel, but with two different substrate temperatures. Sample nr. 2 followed the normal procedure with a substrate temperature of 150 K, while sample nr. 10 had a substrate temperature of 300 K during nickel evaporation. The estimated amount of nickel on the samples after heating is almost the same, 0.56 monolayers of nickel for sample nr. 2 and 0.52 monolayers of nickel for sample nr. 10. The nickel amount before heating is not estimated for sample nr. 2, but is assumed to be around 0.7 monolayers if comparing the values with sample nr. 13. The difference between the nickel amount before and after heating for sample nr. 10 is quite small, and almost negligible, as it decreases from 0.56 to 0.52 monolayers. This small change is probably due to the increased substrate temperature upon evaporation, as the nickel particles can find their stable states when being evaporated.

Figure 4.9 shows the difference between the TPD spectra from 1.0 L, 0.5 L and 0.1 L CO coverage, at substrate temperatures during nickel evaporation of 150 K and 300 K. The rest of the TPD results for the two samples are presented in figure 4.4 and in Appendix A in figure A.6.

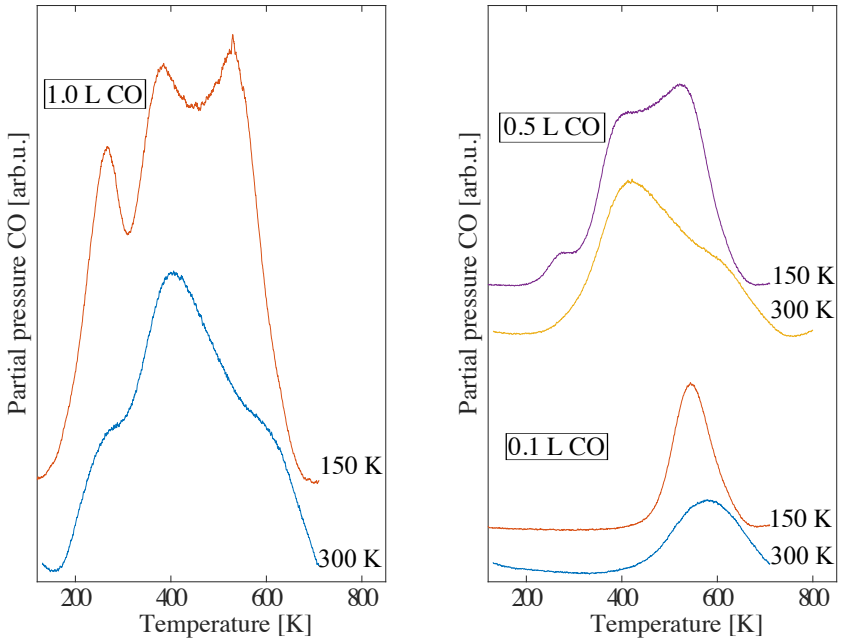

Figure 4.9: TPD spectra showing the difference between CO desorption from samples with different nickel evaporation substrate temperatures. The two substrate temperatures used are 150 K and 300 K. CO coverages of 1.0 L, 0.5 L and 0.1 L are included in the figures.

The desorption energies are quite similar for the two samples, ranging from 0.12 to 1.0 eV for the sample with substrate temperature of 150 K, and from 0.19 to 0.71 eV for the sample with substrate temperature of 300 K. The 150 K sample seems to adsorb a bit more CO than the 300 K sample, as the area under the different desorption spectra is somewhat larger for all the CO coverages. This difference is small, so it is difficult to know if this is a consequence of the variations or just a coincidence.

The biggest difference seems to be in the intensity of the different peaks, as for the other variations in sample preparation presented above. The desorption peaks at 280 K and 550 K are more distinct for the 150 K sample. The small CO coverage curves have quite similar desorption peaks, but the larger CO coverage, the bigger differences are found in the spectra, as the peaks at 280 K and 550 K grow higher for the 150 K sample.

The difference between these two samples can have several explanations. It is natural that there is a difference in surface morphology when varying the substrate temperature during nickel evaporation. When the nickel is evaporated at a substrate temperature of 150 K, the nickel particles will stay where they hit the surface until being heated [33]. This way, the nickel particles will not be in their stable states before the sample is heated and the

particles diffuse on the surface. When the nickel is evaporated at a substrate temperature of 300 K, the particles might diffuse when hitting the surface, finding their stable states immediately. Another possibility is that some of the nickel can move in between the mica layers. This scenario would be more likely at a substrate temperature of 300 K than 150 K. Both of these possibilities can cause differences in the Ni-mica surface morphology, which again causes differences in the CO adsorption.

4.3 AFM

Atomic force microscopy is used to get an image of the surface morphology of the nickel-decorated mica samples. AFM images are taken of three different samples, a small, medium and large nickel dose. The one with the small dose is sample nr. 5, which is estimated to have approximately 0.1 monolayers of nickel on its surface. The one with the medium dose is sample nr. 3, which is estimated to have approximately 0.6 monolayers of nickel on its surface. The one with the large dose is sample nr. 14, which is estimated to have approximately 12.7 monolayers of nickel on its surface before heating, and 4.0 monolayers after heating.

The Ni-mica samples are taken out of the vacuum chamber for AFM imaging. All images are taken after the samples are heated through several CO adsorption and desorption cycles. No image is obtained of the Ni-mica samples before heating, so we cannot say anything about how the nickel is distributed on the surfaces before being heated. The images are taken in peak force tapping mode in air, using a ScanAsyst probe. The mica surface is assumed to be around 0.0 nm in the height scale, at least for the two first images. The negative values are assumed to be because of the tip tapping into the sample.

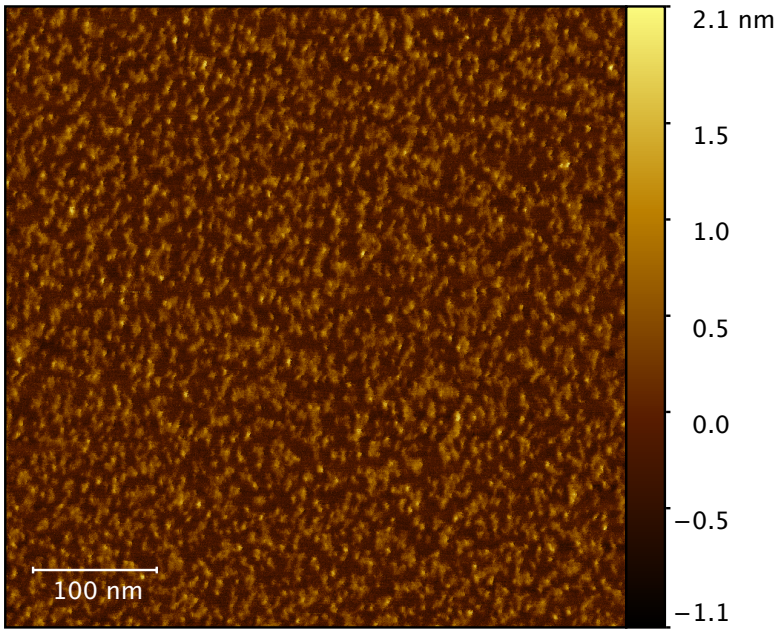

Figure 4.10: AFM image of mica sample nr. 5, covered with approximately 0.1 monolayers of nickel on its surface. The image is 500 × 500 nm, and the dimension is given with the white bar in the down-left corner.

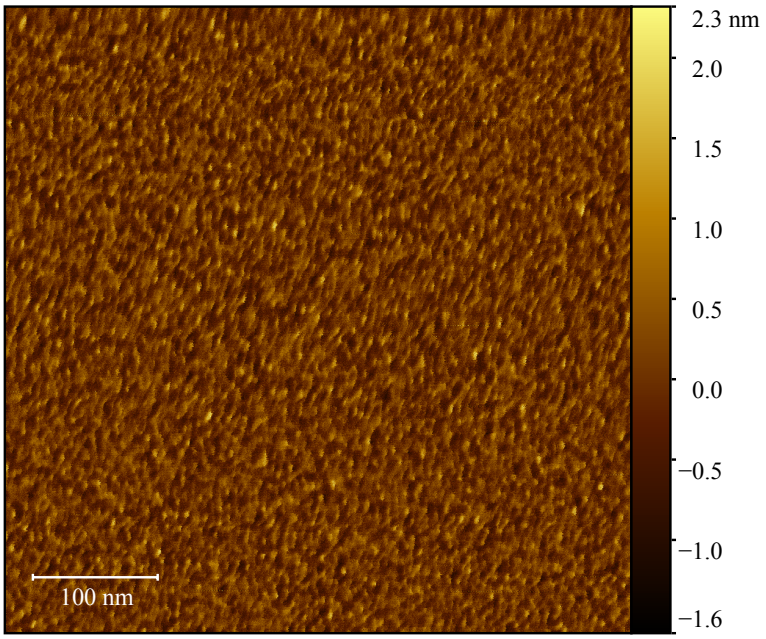

Figure 4.11: AFM image of mica sample nr. 3, covered with approximately 0.6 monolayers of nickel on its surface. The image is 500 × 500 nm, and the dimension is given with the white bar in the down-left corner.

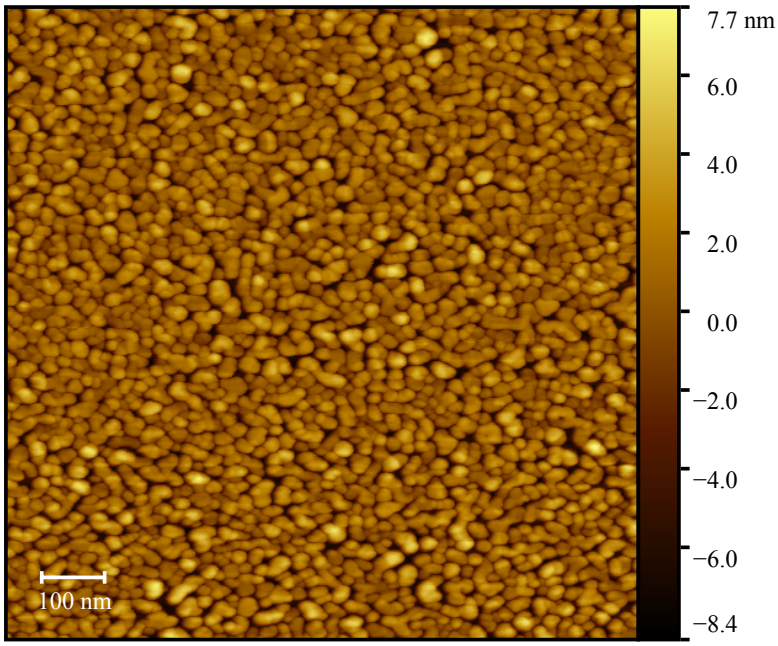

Figure 4.12: AFM image of mica sample nr. 14, covered with approximately 12.7 monolayers of nickel on its surface estimated before heating and 4.0 monolayers of nickel after heating. The image is 1×1 μm, and the dimension is given with the white bar in the down-left corner.

The small and medium covered Ni-mica samples are imaged in figure 4.10 and 4.11, respectively. They both have less than one monolayer of nickel on their surfaces. These surfaces are somewhat similar, with Ni clusters with approximately the same diameter and height. The difference is that the sample with the medium Ni dose, appears to have a higher number of clusters packed closer together.

The sample with the large Ni dose, imaged in figure 4.12, has much more than one monolayer of nickel on its surface. This makes the sample surface look very different from the two other samples. The nickel clusters are much larger, both in diameter and height, and they cover approximately the entire mica surface. During the XPS measurements, it was shown that they do not cover the surface entirely, because the same charge compensation is necessary for this sample as for the samples with small amounts of nickel.

5 Discussion

This chapter includes further discussions of the main results obtained in this work. Some of the results are discussed briefly after being presented in the previous chapter, while the overall trends of the results are discussed here. The first section gives a comment on how the surface morphology changes as a result of heating the sample. The second section is on the effects of varying different parameters in the sample preparation procedure. In the third section, the different desorption peaks found in the TPD spectra are compared to results from earlier studies of CO adsorption on different nickel surfaces. The last section looks at the decomposition of CO on Ni-mica surfaces.

5.1 Changes in surface morphology

It is found that the nickel-decorated muscovite mica surface changes when being heated up to temperatures around 710 K. The XPS results show that the estimated amount of Ni on the surface changes from before to after sample heating. This change in surface morphology is also found to cause changes in the way CO adsorbs on the surface. Both the desorption peaks and the area under the TPD spectrum change from the first to the second 1.0 L CO desorption. Doering and co-workers [10] found that thermal treatments of the Ni-mica sample caused morphological particle changes, accompanied by changes in CO binding energy. In this work, these changes mostly seem to happen during the first heating of the sample. This is assumed because the TPD spectrum for the different subsequent CO coverages shows approximately the same peaks for similar coverages, compared to the difference between the first and second 1.0 L CO coverage.

These results are also obtained in previous work on the same system, so a simple model of the change was presented in the section on XPS data analysis, in section 3.1. It was assumed that the nickel, when first evaporated on the mica sample at low temperatures, appeared as a thin film on the surface, and that this film changes into clusters when being heated. The results obtained in this work support this simple model, as the changes are bigger for the larger Ni doses. The largest Ni dose is estimated to change from approximately 12.7 monolayers to 4.0 monolayers of nickel, which is a decrease of almost 70 %. The smallest Ni dose is estimated to change from 0.1 to 0.08 monolayers of nickel, a decrease of 20 %. For this sample, and the other samples with a small nickel dose, the amount of nickel is far from

enough to make a thin layer covering the mica surface. It is then assumed that the nickel particles are almost separate and cover more of the surface before heating, and diffusing to clusters covering less of the mica surface during the heating.

There might be other reasons for these changes in the estimated amount of nickel on the mica surfaces, one of them being that the nickel particles could move out of the surface edges during heating of the sample. However, the above explanation seems more likely for these samples.

5.2 Variation in sample preparation

The adsorption of CO on the Ni-mica surface is also found to depend on the preparation of the sample. No apparent differences are found between thermal evaporation and electron beam evaporation of nickel on the samples, or as a result of different nickel evaporation rates. There is however found an effect of varying the annealing procedure and the substrate temperature during nickel evaporation.

Consistent for both the variation in annealing procedure and the variation in substrate temperature during nickel evaporation, is that the samples which do not follow the normal procedure get less distinct desorption peaks around 250 K and 550 K. While we do not know why this happens, it is found that the best sample preparation is to anneal the samples at 700 K overnight and evaporate nickel at a substrate temperature of 150 K. The samples prepared this way are found to adsorb more CO than samples prepared differently, the biggest effect coming from a good annealing procedure.

5.3 The different desorption peaks

Three main desorption peaks are found from CO desorption on different Ni-mica samples, around 250-280 K, 350-420 K and 550-600 K. These peaks vary in appearance and size with varying the amount of nickel on the samples, the annealing procedure, and the nickel evaporation temperature. The samples with a small amount of nickel showed a main peak at around 400 K, the samples with a medium amount of nickel showed all the peaks mentioned above, and the samples with a large amount of nickel only showed one desorption peak at around 550 K. The desorption peak temperatures are somewhat difficult to trust completely because of the use of different sample holders which showed different thermal properties. Some of the peaks are assumed to be shifted approximately 30 K towards higher temperatures because of a

bad thermal contact in one of the sample holders, so the temperatures of the peaks are all approximate.

From the results obtained in this work, it is difficult to determine where and how the CO adsorbs on the Ni-mica surfaces. However, some assumptions to what causes the different desorption peaks can be made. Some of the TPD spectra show an additional small desorption peak around 200 K, which seems to be more prominent on the first 1.0 L CO desorption spectrum. This small peak is assumed to be due to water leaving the sample at the same temperature.

The desorption peaks around 250-280 K are reasonably assumed to be due to adsorbate-adsorbate interactions of CO. Earlier work on CO adsorption on metal surfaces using Monte-Carlo simulations found that the shape of the desorption spectrum is more sensitive to variations in adsorbate-adsorbate interactions than to site dependent desorption energies [34]. It was also found that numerical values for lateral interactions for CO on metallic substrates were in the range 0.1 eV and lower. This is consistent with the results obtained here, as the TPD spectra become broader with increased CO coverage. For the samples with a medium nickel dose, desorption energies around 0.1 to 0.3 eV are found for the lowest desorption peaks at around 250-280 K. These peaks are as mentioned assumed to be from lateral interactions, due to the fact that these peaks are the only ones increasing with the largest CO coverages of 2.0, 5.0 and 10.0 L.

A comparison with CO adsorption on stepped Ni surfaces is also relevant, as particulate Ni films can be expected to behave similar to a stepped nickel surface with regard to the adsorption of CO [10]. Earlier studies conducted by Benndorf and Meyer [13, 14] have involved the adsorption of CO on different kinds of stepped Ni surfaces. They studied Ni(551), Ni(331) and Ni(221) surfaces, and found that the CO/Ni binding strength was lowered for CO adsorbed at step sites. They assumed that the low temperature peaks in the CO TPD spectra were because of adsorption on step sites on the surface. They also found a sequential filling of different desorption states with increasing CO coverage, similar to the results obtained in this work for the medium dose Ni-mica surfaces. Ni(111) surfaces only have one desorption peak around 450 K, while the stepped surfaces had several desorption peaks. Ni(331) had peaks at 455 K, 360 K and 218 K, and Ni(221) had peaks at 455 K, 300 K and 250 K. The high temperature desorption peak for the stepped surfaces was assumed to be because of adsorption on terrace sites. Comparing these results to our TPD results, one might assume that the desorption peak around 550 K is due to adsorption on terrace sites, while the desorption peak around 400 K is due to adsorption on step sites. Since the samples with several monolayers of nickel on their surfaces only have one peak around 550

K, the adsorption might only take place at terrace sites on top of the large Ni clusters. For the mica samples with small amounts of nickel, there might not be that many terrace sites, leading to adsorption almost only on step sites, giving the main desorption peak at around 400 K. For the samples with the medium nickel dose, all of the three desorption peaks are present for the largest CO coverages. The peaks at 400 K and 550 K are often quite similar, maybe indicating that there are almost equal amounts of terrace and step sites on these surfaces.

These results are also consistent with results obtained in a study done on the adsorption of CO on polycrystalline nickel films on glass [35]. That study found desorption peaks at 170 K, 310-330 K and 460-490 K, and concluded that this was due to one weakly bound and two chemisorbed species. The small CO coverages only had a peak at 490 K, and the larger the coverage, the more peaks, in agreement with the present work for the medium dose Ni-mica surfaces.

5.4 CO decomposition

The discussion has until now only been about the adsorption of CO as a molecule, but CO can also decompose to a carbon and oxygen atom during the adsorption process. CO decomposition is a key step in a number of catalytic reactions, including the carbon monoxide methanation reaction on nickel [10]. XPS measurements presented in figure 4.3 show that there is some carbon left on the surface after CO adsorption and desorption. Almost all of the Ni-mica samples showed a small carbon peak at the end of the experiment, which might be a result of CO decomposition.

Earlier work on CO adsorption on Ni-mica surfaces, done by Doering, Dickinson and Poppa [10], found that particulate Ni films behave similar to a stepped nickel surface with regard to CO decomposition, and their work focused on the decomposition of CO on the Ni-mica surface. They found that CO decomposes on Ni clusters at a rate strongly dependent on particle size, especially for clusters below 5 nm in diameter. This is said to be because of the high density of edge and corner sites on surfaces with small Ni particles. To desorb the carbon atoms occurring at decomposition of CO, an oxygen exposure was necessary. The CO desorption peak resulting from this was found at about 620 K and 820 K. This was in addition to a standard molecular CO desorption peak around 400 K.

The TPD results obtained in this work do not show any desorption peaks above 550-600 K, but this might have happened if the samples were exposed to oxygen prior to the desorption, and the TPD was run to higher temper-

atures. Since the focus has not been on CO decomposition in this work, missing XPS measurements and not perfectly clean samples makes it difficult to find any difference between the different samples when it comes to CO decomposition. However, since the AFM images of the two samples with the smallest nickel doses show that the nickel clusters are well below 5 nm in diameter, it is reasonable to believe that some CO decomposition does occur on our samples as it did for Doering and co-workers.

6 Conclusion

6.1 Concluding remarks

Adsorption of carbon monoxide on nickel-decorated muscovite mica has been studied using the surface analysis techniques XPS, TPD and AFM.

CO was adsorbed at nickel-decorated muscovite mica, with various amounts of nickel deposited on the mica surfaces. Desorption peaks are found in three main regions, around 250-280 K, 350-420 K and 550-600 K. The intensity of the peaks is found to vary with the amount of nickel on the mica surfaces, and with the preparation procedure.

The results show that the sample preparation procedure is of importance for CO adsorption, especially the annealing procedure. Mica surfaces annealed at 700 K overnight, prior to Ni and CO exposures at substrate temperatures of 150 K were found to adsorb the largest amounts of CO.

Desorption energies and corresponding pre-exponential factors are calculated for the different desorption spectra. Desorption energies were found in the range 0.1 to 1.25 eV, and the pre-exponential factors were found in the range 1 to $10^{8.5}$ s^{-1}, varying with CO coverage and various Ni-mica surfaces.

XPS measurements show some evidence of CO decomposition on our samples. A small increase in the carbon peak is found for some of the samples after CO adsorption and desorption. Comparing with earlier studies, this carbon might desorb if the surfaces are exposed to oxygen prior to desorption, at temperatures around 620 K and 820 K.

6.2 Outlook

This work has shown that the Ni-mica system is quite complex. The decomposition of carbon monoxide on the Ni-mica surfaces can be studied more closely, by trying to introduce oxygen gas to the surfaces and doing temperature programmed desorption to higher temperatures. In addition, more work could be done with the atomic force microscope. Only a small selection of samples were imaged in this work, and not much time was spent analysing the obtained images. It is also a possibility to evaporate even larger doses of nickel on the mica surface. It can be interesting to see if this can lead to a continuous nickel film which will not need charge compensation when doing X-ray photoelectron spectroscopy, and if this will give different TPD spectra from the ones obtained here.

References

[1] Siriwardane, R., Shen, M., Fisher, E., Poston, J. & Shamsi, A. Adsorption and Desorption of CO on Solid Sorbents. *Carbon* **2,** 2 (2015).

[2] Hemmen, H. *et al.* X-ray studies of carbon dioxide intercalation in Na-fluorohectorite clay at near-ambient conditions. *Langmuir* **28,** 1678–1682 (2012).

[3] Giesting, P., Guggenheim, S., van Groos, A. F. K. & Busch, A. Interaction of carbon dioxide with Na-exchanged montmorillonite at pressures to 640 bars: Implications for CO_2 sequestration. *International Journal of Greenhouse Gas Control* **8,** 73–81 (2012).

[4] Hu, Z.-P., Weng, C.-C., Yuan, G.-G., Lv, X.-W. & Yuan, Z.-Y. Ni nanoparticles supported on mica for efficient decomposition of ammonia to COx-free hydrogen. *International Journal of Hydrogen Energy.* ISSN: 0360-3199 (2018).

[5] Li, P. *et al.* High efficient nickel/vermiculite catalyst prepared via microwave irradiation-assisted synthesis for carbon monoxide methanation. *Fuel* **171,** 263–269 (2016).

[6] Gao, J. *et al.* Ni/Al2O3 catalysts for CO methanation: Effect of Al2O3 supports calcined at different temperatures. *Journal of Energy Chemistry* **22,** 919–927 (2013).

[7] Poppa, H. & Elliot, A. G. The surface composition of mica substrates. *Surface Science* **24,** 149–163 (1971).

[8] Van der Heide, P. *X-ray photoelectron spectroscopy: an introduction to principles and practices* (John Wiley & Sons, 2011).

[9] Ostendorf, F. *et al.* How flat is an air-cleaved mica surface? *Nanotechnology* **19,** 305705 (2008).

[10] Doering, D., Dickinson, J. & Poppa, H. UHV studies of the interaction of CO with small supported metal particles, NiMica. *Journal of Catalysis* **73,** 91–103 (1982).

[11] Netzer, F. P. & Madey, T. E. The structure of CO on Ni (111). *The Journal of Chemical Physics* **76,** 710–715 (1982).

[12] Christmann, K., Schober, O. & Ertl, G. Adsorption of CO on a Ni (111) surface. *The Journal of Chemical Physics* **60,** 4719–4724 (1974).

[13] Benndorf, C. & Meyer, L. CO adsorption on stepped Ni (111) surfaces. *Journal of Vacuum Science & Technology A: Vacuum, Surfaces, and Films* **8,** 2677–2681 (1990).

[14] Benndorf, C. & Meyer, L. CO adsorption on Ni (551). *Surface Science* **251,** 872–876 (1991).

[15] Venables, J., Spiller, G. & Hanbucken, M. Nucleation and growth of thin films. *Reports on Progress in Physics* **47,** 399 (1984).

[16] Reinbold, M. & Hoffmann, H. Determination of orientation of small crystallites in thin nickel films on UHV-cleaved mica. *Thin Solid Films* **32,** 367–369 (1976).

[17] Winau, D., Koch, R. & Rieder, K. Growth mode related intrinsic stress of thin nickel and iron films under the influence of oxygen. *Vacuum* **43,** 525–527 (1992).

[18] Ratner, B. D. & Castner, D. G. *Surface Analysis: The Principal Techniques* (Wiley: Chichester, England, 1997).

[19] O'Connor, J., Sexton, B. & Smart, R. S. *Surface analysis methods in materials science* (Springer, 1992).

[20] Zangwill, A. *Physics at surfaces* (Cambridge university press, 1988).

[21] Yates, J. T. in *Methods of Experimental physics* (eds Park, R. L. & Lagally, M. G.) 425–464 (Academic Press, 1985).

[22] Woodruff, D. & Delchar, T. *Modern techniques of surface science* (Cambridge University Press, 1986).

[23] Rakić, V. & Damjanović, L. in *Calorimetry and Thermal Methods in Catalysis* 131–174 (Springer, 2013).

[24] Van Bramer, S. E. An introduction to mass spectrometry. *Widener University, Department of Chemistry, One University Place, Chester, PA* **19013** (1997).

[25] Eaton, P. & West, P. *Atomic force microscopy* (Oxford University Press, 2010).

[26] Haugstad, G. *Atomic force microscopy: understanding basic modes and advanced applications* (John Wiley & Sons, 2012).

[27] Kaemmer, S. B. Introduction to Bruker's ScanAsyst and PeakForce Tapping AFM Technology.

[28] Foster, B. New Atomic Force Microscopy(AFM) Approaches Life Sciences Gently, Quantitatively, and Correctively. *American laboratory* **44,** 24–28 (2012).

[29] Moore, J. H., Davis, C. C., Coplan, M. A. & Greer, S. C. *Building scientific apparatus* (Cambridge University Press, 2009).

[30] Ibach, H. *Physics of surfaces and interfaces* 94–95 (Springer, 2006).

[31] Smith Jr, J. N. & Fite, W. L. Reflection and Dissociation of H2 on Tungsten. *The Journal of Chemical Physics* **37,** 898–904 (1962).

[32] Song, Y., Lu, Q. & Gong, X. Mechanism and model of atomic hydrogen cleaning for different types of carbon contamination on extreme ultraviolet multilayers. *Thin Solid Films* **612,** 96–100 (2016).

[33] Henry, C. R. Surface studies of supported model catalysts. *Surface Science Reports* **31,** 231–325 (1998).

[34] Raaen, S. & Ramstad, A. Monte-Carlo simulations of thermal desorption of adsorbed molecules from metal surfaces. *Energy* **30,** 821–830 (2005).

[35] Wedler, G., Papp, H. & Schroll, G. Adsorption of carbon monoxide on polycrystalline nickel films. *Surface Science* **44,** 463–479 (1974).

A Additional results

In this appendix, the additional results from the TPD experiments are presented. The nickel amounts estimated on the different samples are presented in table 4.1 in the result chapter. Unless otherwise stated, the samples are cleaved with scotch tape, annealed at 700 K overnight and hydrogen treated, prior to Ni and CO exposure at a substrate temperature of 150 K.

Sample nr. 5

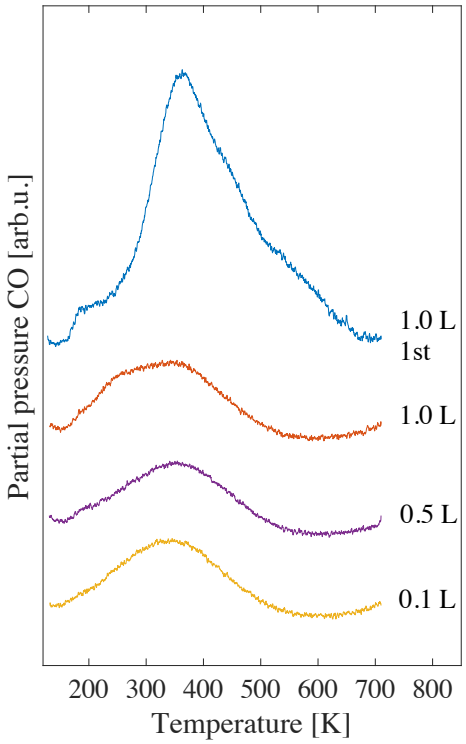

Figure A.1: TPD spectra of CO on 0.1 monolayers of nickel on mica. The CO exposure is given in the figure. Ni was deposited by thermal evaporation. The top spectrum represents the first run, and the other spectra are subsequent runs. The temperature ramp was 1 K/s.

Figure A.1 shows the TPD spectra of CO on 0.1 monolayers of nickel on mica. The main desorption peak is around 350 K, with a shoulder towards 250 K. Because of the broad and blurry peaks, no kinetic desorption parameters were obtained for this sample. The surface of this sample is shown in the AFM image in figure 4.10, in the results chapter.

Sample nr. 6

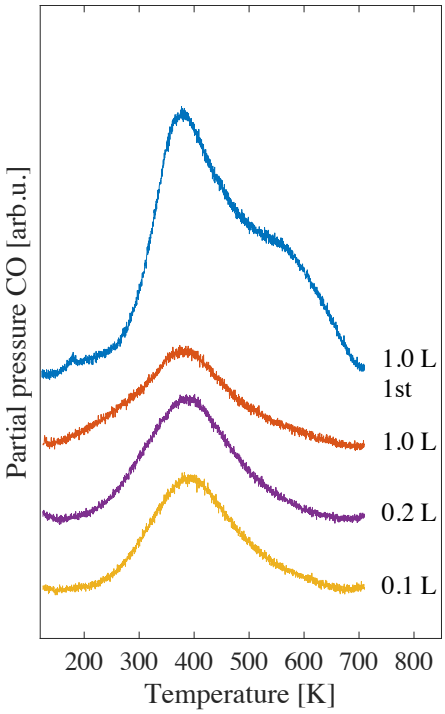

(a) TPD spectra from CO on Ni-mica

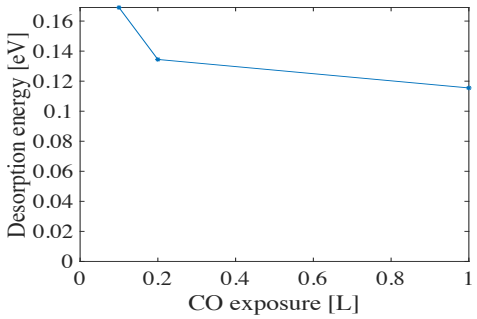

(b) Variation in desorption energy with coverage

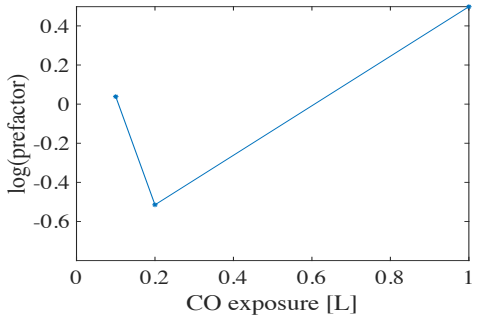

(c) Variation in prefactor with coverage

Figure A.2: (a) TPD spectra of CO from 0.23/0.16 monolayers of nickel on mica. The CO exposure is given in the figure. Ni was deposited by thermal evaporation. The top spectrum represents the first run, and the other spectra are subsequent runs. The temperature ramp was 1 K/s. (b) and (c) Desorption energy and pre-exponential factor as a function of CO coverage.

Figure A.2 shows the TPD spectra from 0.23/0.16 monolayers of nickel on mica, along with the kinetic desorption parameters. The main desorption peak is found around 400 K, and the spectra broaden towards 280 K and 550 K. The desorption energies are quite small, in the range 0.17 to 0.12 eV, indicating that the CO is loosely bound to the Ni-mica surface. The corresponding pre-exponential factors are approximately 1 s^{-1}.

Sample nr. 7

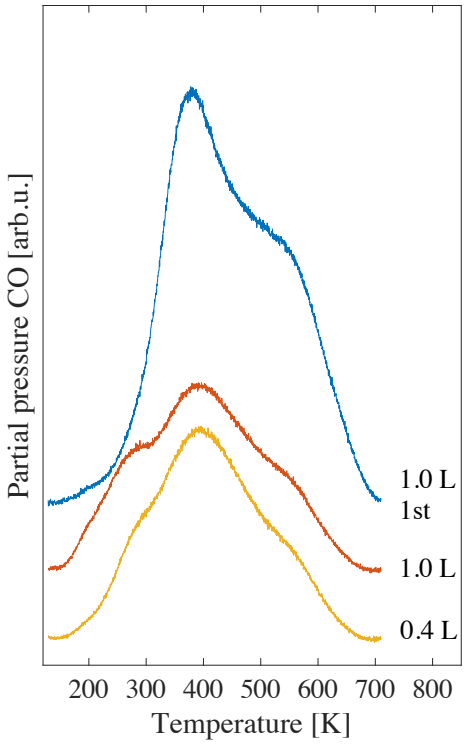

Figure A.3: TPD spectra of CO from 0.37 monolayers of nickel on mica, annealed at 600 K for one hour. The CO exposure is given in the figure. Ni was deposited by thermal evaporation. The top spectrum represents the first run, and the other spectra are subsequent runs. The temperature ramp was 1 K/s.

Figure A.3 shows the TPD spectra of CO on 0.37 monolayers of nickel on mica. The mica sample was only annealed at 600 K for one hour prior to Ni and CO exposure. The main desorption peak is around 400 K, with two additional peaks around 280 K and 550 K. The desorption energy was found to be 0.19 eV for 1.0 L CO and 0.14 eV for 0.4 L CO. The corresponding pre-exponential factors were 3 and 1 s^{-1}, respectively.

A decrease in area from the first to the second 1.0 L CO desorption spectrum was found to be around 49 %.

Sample nr. 8

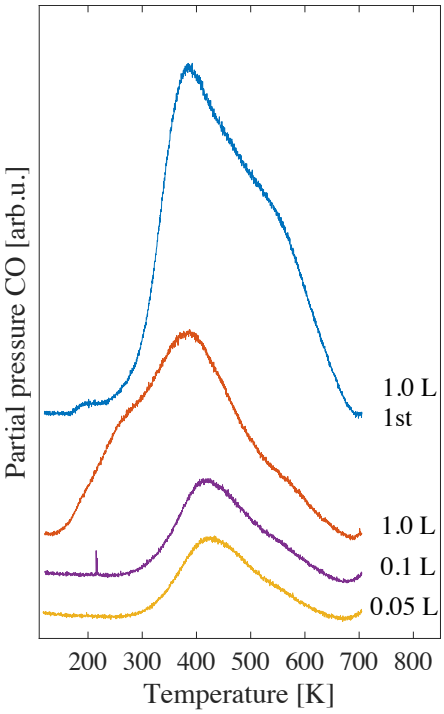

(a) TPD spectra from CO on Ni-mica

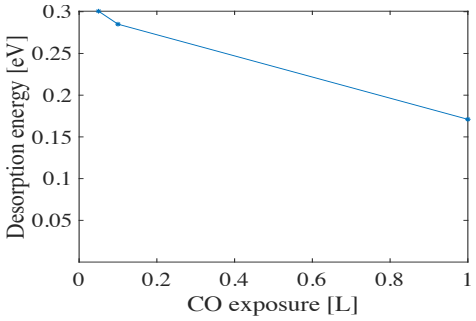

(b) Variation in desorption energy with coverage

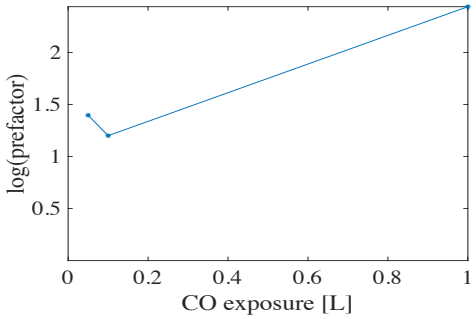

(c) Variation in prefactor with coverage

Figure A.4: (a) TPD spectra of CO from 0.53 monolayers of nickel on mica, annealed at 600 K overnight. The CO exposure is given in the figure. Ni was deposited by thermal evaporation. The top spectrum represents the first run, and the other spectra are subsequent runs. The temperature ramp was 1 K/s. (b) and (c) Desorption energy and pre-exponential factor as a function of CO coverage.

Figure A.4 shows the TPD spectra of CO on 0.53 monolayers of nickel on mica, along with the kinetic desorption parameters. The mica sample was annealed at 600 K overnight prior to Ni and CO exposure. The main desorption peak is around 390 to 420 K. For all of the CO coverages, the spectra broaden towards 550 K, and for the 1.0 L CO coverage, the spectrum also shows a peak at around 250 K. The desorption energy is found in the range 0.3 to 0.17 eV, with corresponding pre-exponential factors around $10^{1.3}$ to $10^{2.5}$ s^{-1}.

The area under the 1.0 L CO desorption spectrum decreases with 36 % from the first to the second run.

Sample nr. 9

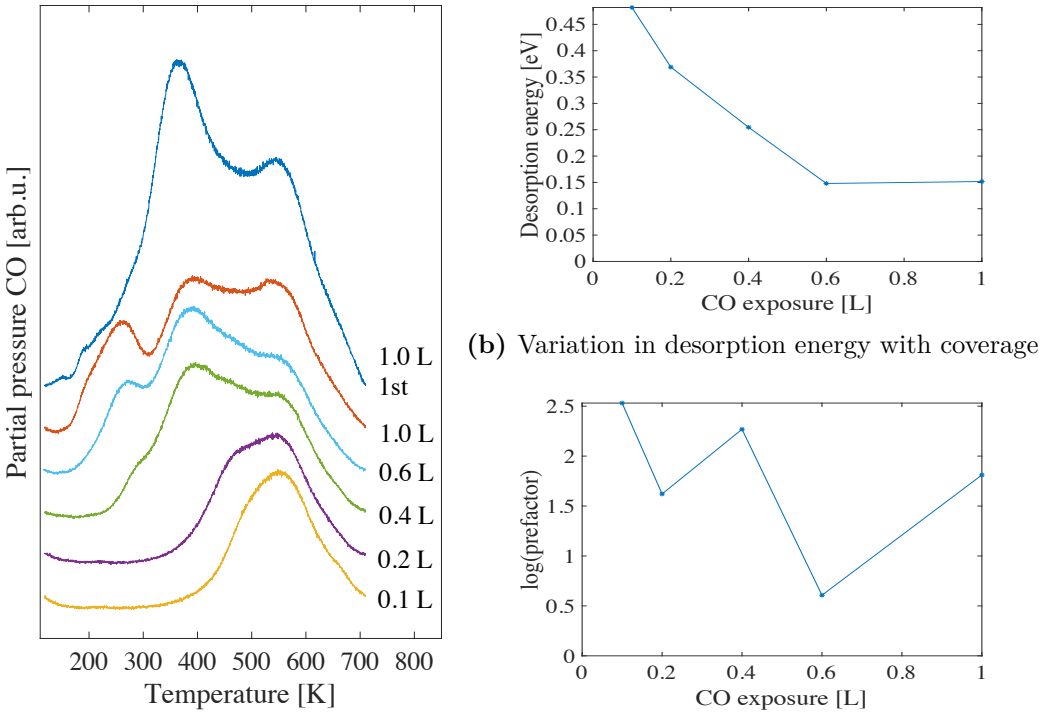

(a) TPD spectra from CO on Ni-mica

(b) Variation in desorption energy with coverage

(c) Variation in prefactor with coverage

Figure A.5: (a) TPD spectra of CO from 0.5 monolayers of nickel on mica. The CO exposure is given in the figure. Ni was deposited by thermal evaporation. The top spectrum represents the first run, and the other spectra are subsequent runs. The temperature ramp was 1 K/s. (b) and (c) Desorption energy and pre-exponential factor as a function of CO coverage.

Figure A.5 shows the TPD spectra of CO on 0.5 monolayers of nickel on mica, along with the kinetic desorption parameters. The main desorption peaks are around 550 K, 380 K and 250 K. All of the CO coverages have a desorption peak at 550 K. With increased CO coverage, the peaks at 380 K and 250 K also increase. The desorption energies are found in the range 0.5 to 0.15 eV, with corresponding pre-exponential factors in the range $10^{2.5}$ to $10^{0.5}$ s^{-1}.

The area of the 1.0 L CO desorption spectrum decreases with about 39 % from the first to the second run.

Sample nr. 10

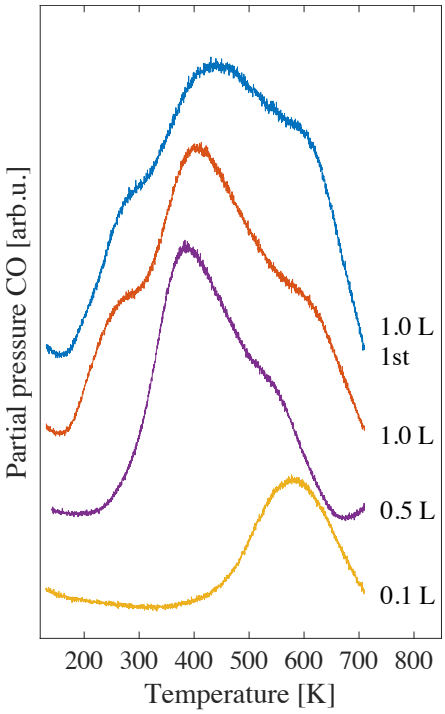

(a) TPD spectra from CO on Ni-mica

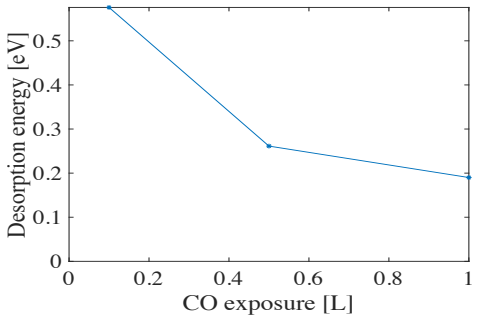

(b) Variation in desorption energy with coverage

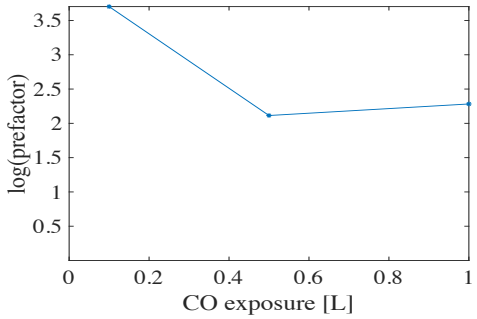

(c) Variation in prefactor with coverage

Figure A.6: (a) TPD spectra of CO from 0.56/0.52 monolayers of nickel on mica, with nickel deposited by thermal evaporation at substrate temperatures of 300 K. The CO exposure is given in the figure. The top spectrum represents the first run, and the other spectra are subsequent runs. The temperature ramp was 1 K/s. (b) and (c) Desorption energy and pre-exponential factor as a function of CO coverage.

Figure A.6 shows the TPD spectra of CO on 0.56/0.52 monolayers of nickel on mica. The mica sample followed the usual annealing procedure, but nickel was deposited at a substrate temperature of 300 K prior to CO exposure at a substrate temperature of 150 K. All of the CO coverages have a desorption peak at 550-600 K. The 0.5 L and 1.0 L CO coverages also have a peak around 400 K, and the 1.0 L CO coverage has an additional peak around 250 K. The desorption energy ranges from 0.6 to 0.2 eV, with corresponding pre-exponential factors in the range $10^{3.7}$ to $10^{2.1}$ s^{-1}.

The estimated amount of nickel on the mica surface had a small decrease after heating, compared to the other Ni-mica samples. The decrease in area from the first to the second 1.0 L CO desorption spectrum was approximately 17 %.

Sample nr. 11

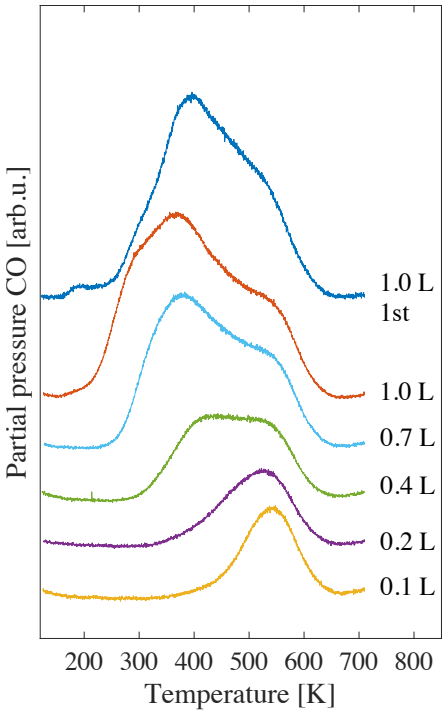

(a) TPD spectra from CO on Ni-mica

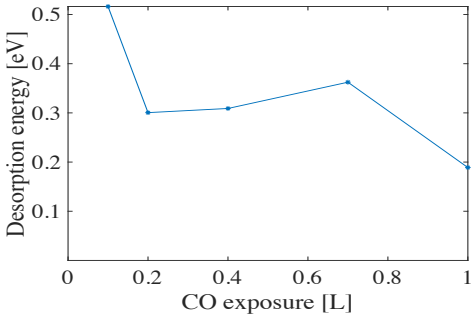

(b) Variation in desorption energy with coverage

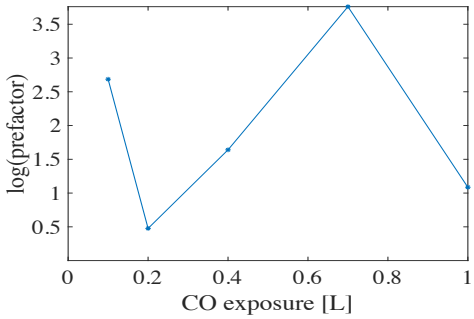

(c) Variation in prefactor with coverage

Figure A.7: (a) TPD spectra of CO from 1.28/1.01 monolayers of nickel on mica. The CO exposure is given in the figure. Ni was deposited by thermal evaporation. The top spectrum represents the first run, and the other spectra are subsequent runs. The temperature ramp was 1 K/s. (b) and (c) Desorption energy and pre-exponential factor as a function of CO coverage.

Figure A.7 shows the TPD spectra of CO from 1.28/1.01 monolayers of nickel on mica. All of the CO coverages show a desorption peak around 550 K, with an increasing peak around 380 K with increasing CO coverage. The 1.0 L CO desorption spectrum also has a shoulder around 250 K. The desorption energy is in the range 0.5 to 0.2 eV, with corresponding pre-exponential factors in the range $10^{3.7}$ to $10^{0.5}$ s^{-1}. The pre-exponential factor did not follow the same CO coverage dependent curve as the desorption energy.

For this Ni-mica surface, the area of the 1.0 L CO desorption spectrum did not show a significant change between the first and the second run. The area was somewhat larger for the second run, which is different from the other results.

Sample nr. 12

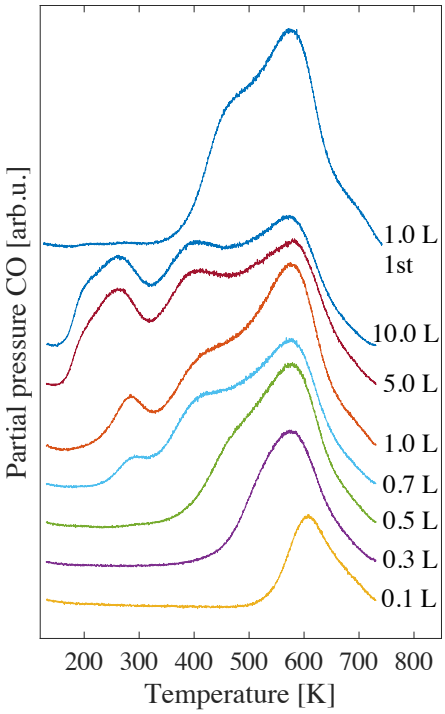

(a) TPD spectra from CO on Ni-mica

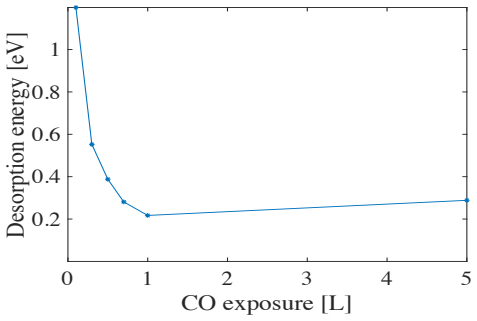

(b) Variation in desorption energy with coverage

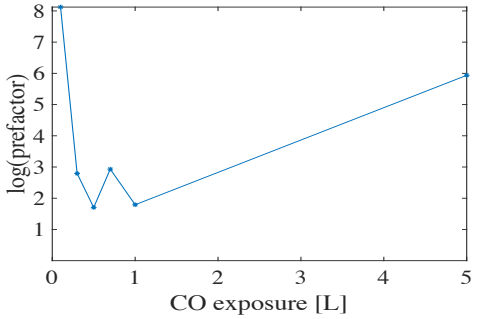

(c) Variation in prefactor with coverage

Figure A.8: (a) TPD spectra of CO from 0.72/0.5 monolayers of nickel on mica. The CO exposure is given in the figure. Ni was deposited by electron beam evaporation. The top spectrum represents the first run, and the other spectra are subsequent runs. The temperature ramp was 1 K/s. (b) and (c) Desorption energy and pre-exponential factor as a function of CO coverage.

Figure A.8 shows the TPD spectra of CO on 0.72/0.5 monolayers of nickel on mica. All of the CO coverages have a desorption peak around 600 K. When the CO coverage is increased, additional peaks appear and increase around 400 K and 250 K. The desorption energy is found in the range 1.2 to 0.2 eV, with corresponding pre-exponential factors in the range 10^8 to $10^{1.7}$ s^{-1}.

The area of the 1.0 L CO desorption spectrum is approximately the same for the first and the second run.

Sample nr. 13

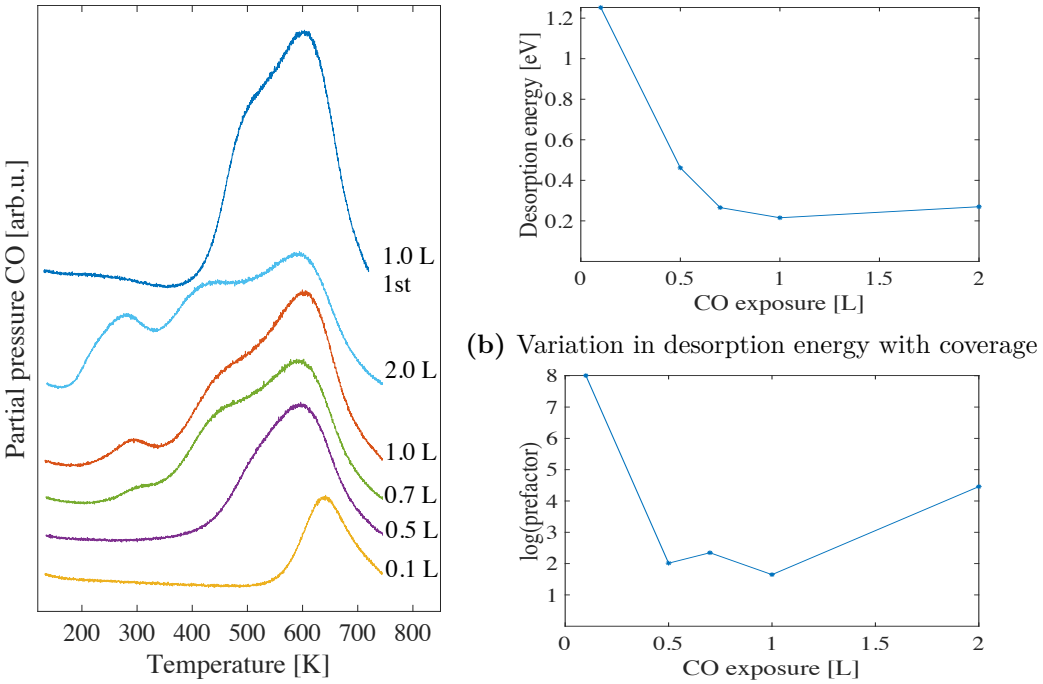

(a) TPD spectra from CO on Ni-mica

(b) Variation in desorption energy with coverage

(c) Variation in prefactor with coverage

Figure A.9: (a) TPD spectra of CO from 0.8/0.7 monolayers of nickel on mica. The CO exposure is given in the figure. Ni was deposited by electron beam evaporation, at half the evaporation rate of sample nr. 12. The top spectrum represents the first run, and the other spectra are subsequent runs. The temperature ramp was 1 K/s. (b) and (c) Desorption energy and pre-exponential factor as a function of CO coverage.

Figure A.9 shows the TPD spectra of CO on 0.8/0.7 monolayers of nickel on mica. This sample was prepared the same way as sample nr. 12, expect that the nickel was evaporated with half the rate as for sample nr. 12. This show that the nickel evaporation rate did not have a significant effect on the CO adsorption. All of the CO coverages show a desorption peak around 600 K, with increasing peaks around 400 K and 280 K with increasing CO coverage. The desorption energies and the corresponding pre-exponential factors were also found in the same range as sample nr. 12, being 1.25 to 0.2 eV and 10^8 to $10^{1.6}$ s^{-1}, respectively.

For this Ni-mica surface, the area of the 1.0 L CO desorption spectrum decreased with 19 % from the first to the second run.

Sample nr. 14

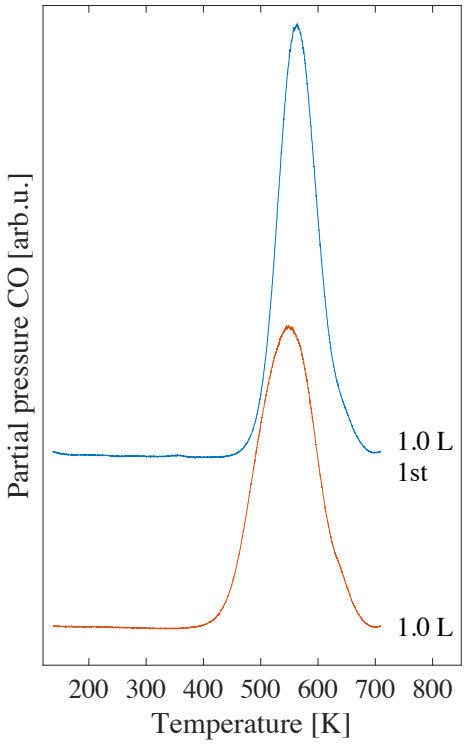

Figure A.10: TPD spectra of CO from 12.7/4.00 monolayers of nickel on mica. The CO exposure is given in the figure. Ni was deposited by electron beam evaporation. The top spectrum represent the first run, and the other spectrum represents a subsequent run. The temperature ramp was 1 K/s.

Figure A.10 shows the TPD spectra of CO on 12.7/4.0 monolayers of nickel on mica. This surface only showed one CO desorption peak around 550 K. The desorption energy for the second 1.0 L CO desorption was 0.8 eV, with a corresponding pre-exponential factor around 10^6 s^{-1}.

The area under the 1.0 L CO desorption peak was approximately the same for the first and the second run.

List of Figures